People's Democratic Republic of Algeria
Ministry of Higher Education and Scientific Research

University M'Hamed BOUGARA – Boumerdes

Institute of Electrical and Electronic Engineering

Department of Power and Control

Final Year Project Report Presented in Partial Fulfilment of the Requirements for the Degree of the

MASTER

In **Power Engineering**

Option: **Power Engineering**

Title:

Simulation and Implementation of MPPT Techniques in a PV System

Presented by:

- **DAHILI Hamza**
- **KHERRA Oussama**

Main-Supervisor:

Pr. BENTARZI Hamid

Co-Supervisor:

Dr. BENDIB Boualem

Registration Number:……/2023

Abstract

Solar power,a clean renewable resource with zero emission unlike the fossil generated electricity and has a tremendous potential of energy which can be harvested using solar panels to be available for industrial and domestic use .The extraction of maximum power with changing environmental conditions is one of the significant concerns with photovoltaic(PV) systems,therefore using MPPT techniques is essential to keep the extracted power as close as possible to the maximum power .This report presents a comparative study between maximum power point tracking (MPPT) methods in Matlab/Simulink program that are perturb-and-observe, incremental conductance ,fractional short circuit current and fractional open circuit voltage . Starting by designing a Pv system and sizing all the necessary components to build the buck converter circuit that is used as an interface to charge a lead acid battery .The control of the system is established by the MPPT techniques at different solar-radiation and temperature levels . Finally the simulations result are presented.

Keywords:photovoltaic systems, maximum power point tracking, fractional short circuit current and fractional open circuit voltage ,MATLAB/SIMULINK,PROTEUS .

Dedication

This thesis is dedicated to the loving memory of my beloved father peace be upon him .Throughout my life ,he was a constant source of inspiration and support .I know that he would be proud of my accomplishments .Also my mother who has been my constant pillar of support for me and for all my family her guidance , encouragement and her belief in my a abilities gave me the confidence to achieve anything i want .I will always be grateful for them.

To my siblings and my sister-in-law who have been my companions and gave me the encouragement to pursue my academic journey. Thank you for everything .

Finally , i dedicate this to all my friends who i have shared with them this amazing period of my life.

Hamza

I have a great pleasure to dedicate this work To my beloved parents, whose endless love, support, and encouragement have been guiding light. Your unwavering belief in me has given me the strength to pursue my dreams.

To my incredible siblings, Your constant support, understanding, and friendship have been there for me through the toughest times. I am truly grateful for your inspiration. Thank you for always being by my side.

Furthermore, I dedicate this to my dear friends who made my university experience unforgettable. Thank you for the laughter, the adventures, and the memories we share. Forever grateful for our friendship.

Oussama

Acknowledgment

*First of all, we are grateful to almighty **ALLAH** for giving us strength and ability to understand, learn and complete this project.*

*We wish to express our sincere thanks to **Dr.BENDIB,Boualem** for his competent guidance and support.*

We would like to express our appreciation to the staff of UDES/EPST CDER(Bouismail) for their valuable contributions and support during the course of our research. Their assistance and cooperation were very helpful in the successful completion of this project.

*We would like also to acknowledge our professor **Pr.BENTARZI,Hamid** for his valuable suggestions and guidance in the preparation of this project.*

We take this opportunity to record our sincere thanks to all IGEE teachers, students, library staff and security service for their valuable help.

We must express our profound gratitude to our parents, family and friends for providing us with unfailing support and continuous encouragement throughout our years of study and through the process of researching and writing this thesis. This accomplishment would not have been possible without them,thank you.

Finally, we also place on record our sense gratitude to all who directly or indirectly have lent their helping hand in this project.

List of Figures

List of Tables

List of abbreviations

AC: Alternating Current

AI: Artificial Intelligence

ANN: Artificial Neural Network

CCM: Continuous Conduction Mode

D: Duty cycle

DCM: Discontinuous Conduction Mode

DOD: Depth Of Charge

EPS: Emergency Power Supply

ESR: Equivalent Series Resistance

Eg: Bandgap(1.12eV)

fs: Switching frequency

FF: Fill Factor

FOCV: Fractional Open Circuit Voltage

FSCC: Fractional Short Circuit Current

G: Irradiance [W/m^2]

HO: High side gate drive output

$\mathbf{I_d}$**:** Diode current

$\mathbf{I_{ph}}$**:** Photo-current

$\mathbf{I_0}$**:** Diode reverse saturation current

$\mathbf{I_{sc}}$**:** Short circuit current

$\mathbf{I_{mpp}}$**:** Current at maximum power point

$\mathbf{I_{pv,n}}$**:** Light generated current at nominal conditions

$\mathbf{I_L}$: Inductor current

$\mathbf{I_c}$: Capacitor current

$\mathbf{I_{Load}}$: Load current

$\mathbf{I_{Switch}}$: Switch current

$\mathbf{I_{qbs}}$: Quiescent current for the high side driver

IC: Incremental Conductance

IC: Integrated circuit

IDE: Integrated Development Environment

K: Boltzmann constant [$1.3806503 \times 10^{-}23$]

K_i: Short circuit current temperature coefficient

K_v: Open circuit voltage temperature coefficient

L_c: Critical inductance

LO: Low side gate drive output

K_{sc}: FSCC factor

K_{oc}: FOCV factor

MPP: Maximum Power Point

MPPT: Maximum Power Point Tracking

N_p: Number of parallel connected cells

PIV: Peak Inverse Voltage

P&O: Perturb and Observe

PSO: Partial Shading Optimization

PWM: Pulse Width Modulation

q: Electron charge $1.60217646 \times 10^{-}19$

Q_{LS}: Level shift charge

Q_g: Gate charge of the MOSFET

Q_{gd}: Gate-to -drain (Miller)charge

STC: Standards Test Conditions

T: Temperature in kelvin

T_s: Switching period

T_{ON}: ON time

T_{OFF}: OFF time

V_{ls}: Voltage drop across side MOSFET

$V_{gs(th)}$): Gate-to-source threshold voltage

Contents

General Introduction:

Due to the development of modern technology, renewable energy is currently the subject that receives the most attention worldwide mostly because of the global energy crisis. As a result, the research for green energy has introduced us to a variety of renewable energy sources. The concept covers electricity produced by renewable energy sources like solar, wind, water, biomass, and geothermal energy. The most secure alternative as a dependable power source among them is solar energy because it is abundant in nature and does not pose any danger to the environment.

There exist a unique point known as Maximum Power Point (MPP) and operating at this point is crucial for maximizing the energy harvested from a solar panel. Maximum power point tracking (MPPT) algorithms are used to continuously adjust the operating conditions of the solar panel, typically by varying the voltage , current,or duty cycle to ensure that it operates as close as possible to the MPP.

There are various factors that can influence the performance of solar cell, such as temperature and irradiance which could affect to the non-linearity of the I-V curve .Therefore,the efficiency of the solar panel will be greatly affected.Using the suitable MPPT algorithm for the specified need is important for better performances .

The purpose of the project would be to study different MPPT algorithms in code form and have a comparision between them.Modeling of the PV panel in Simulink/Simscape to interface it with a designed buck converter that is controlled by MPPT techniques for charging a lead acid battery .After simulation using both MATLAB and PROTEUS the objective is to implement the system on a hardware setup using arduino uno microcontroller.

The organization of the study is as follows:

Chapter1:introduces the PV power generation system as well as the history of the MPPT techniques and introduces different topologies of DC-DC converter.

Chapter2: provide the designing and sizing of the different circuits of the system ,and the working principal of the MPPT algorithms .

Chapter3: it focuses on the simulation of the PV system that is controlled by the proposed codes for charging the battery .

Chapter4:it presents the components used in implementation and the hardware setup.

Finally, a conclusion of the thesis is presented. Moreover, potential research ideas for future work in this field are proposed.

Chapter 1

Overview of Photovoltaic system

1.1 Introduction

PV system is increasingly preferred by developed countries due to its ability to convert the most available and cost-free form of energy into electricity . Additionally, it does not cause any harmful pollution to the environment, which is unlike other known forms of nonrenewable energy production techniques like fossil fuel, hydroelectric, or nuclear energy plants, but the conversion process is weak during cloudy conditions and stops completely at dusk until dawn. It is worth noting that PV panels do not have the capacity to store electricity, but energy can be stored using batteries. Since the PV is highly nonlinear, a special type of power converter called maximum power point tracking (MPPT) converter is used to maximize the power generated from the PV panel and connect it to the grid or the load. The MPPT converter commonly consists of 2 parts: the MPPT algorithm and converter.

This chapter introduces photovoltaic (PV) power generation system. The characteristics of the PV panels and modeling of the PV cell are discussed. The principles of Maximum Power Point Tracking (MPPT) are described. The chapter concludes with defining what is a DC-DC converter and the types that are commonly used.

1.2 Photovoltaic Technology:

1.2.1 Photovoltaic Cell:

A PV cell, also known as a photovoltaic cell, converts light energy to electrical energy by absorbing sunlight. The cell is designed to maximize the surface area exposed to irradiance, which results in increased voltage generation across its two terminals. It is composed of a p-n junction diode made from a semiconductor material and a thin layer of p-type material with a glass window on top. This design allows photons from incident light to easily reach the p-n junction. While silicon and germanium are the most commonly used semiconductor materials for solar cells, gallium arsenide, indium arsenide, and cadmium arsenide are also becoming more used [1].

1.2.1.1 Working Principle:

The solar cell shown in figure 1.1 operates based on the photovoltaic effect principle. During the photovoltaic effect, light penetrates the p-n junction with ease through the thin p-type layer. The energy from the light, in the form of photons, provides enough energy to the junction to create electron-hole pairs. This light breaks the thermal equilibrium of the junction, allowing free electrons to move quickly to the n-type side, and holes to the p-type side of the depletion region. However, once the newly created free electrons come to the n-type side, they cannot cross the junction due to the barrier potential of the junction. Similarly, newly created holes on the p-type side cannot cross the junction due to the same barrier potential. As the concentration of electrons increases on one side (the ”n-type” side) and the concentration of holes increases on the other side (the ”p-type” side), the p-n junction behaves like a tiny battery cell, generating a voltage known as photo-voltage. If a small load is connected across the junction, a small current will flow through it [2].

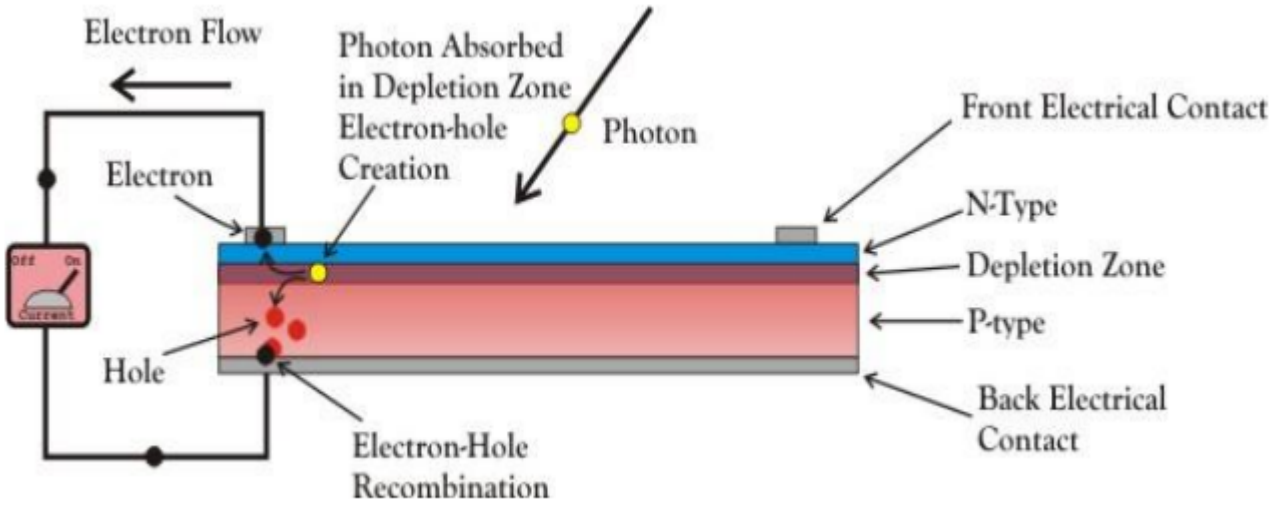

Figure 1.1: PV cell working principle.

1.2.2 PV Module and Array:

To increase the utility of individual PV cells, they are often interconnected together in sealed, weatherproof modules. These modules can then be wired together in series and parallel to create a PV array capable of producing the desired voltage and current. This modular design

provides flexibility to designers to create solar power systems that can meet a wide range of electrical needs.

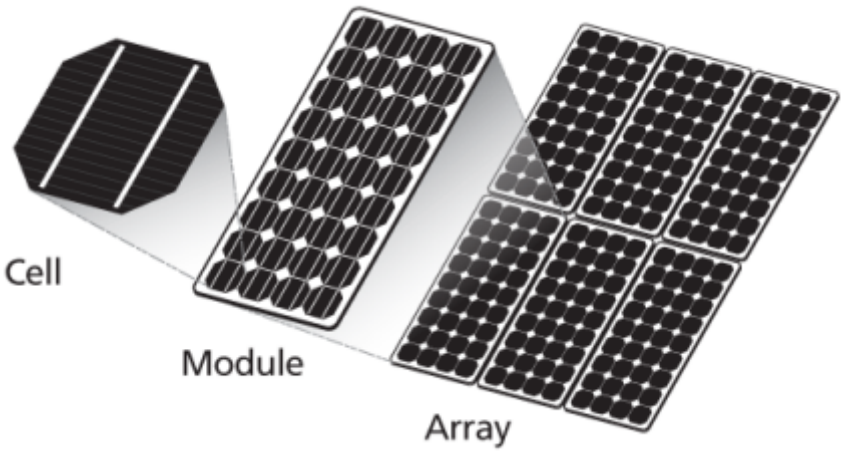

Figure 1.2: PV cell, Module and Array [3]

1.3 PV Modeling:

To accurately predict the power output of solar modules and plot the current-voltage (I-V) characteristics, it is essential to create a model of the solar cell. One commonly used model is the single-diode model, as shown in figure 1.3. This model consists of a photo-current source (I_{ph}), a diode, a series resistor (R_s), and a shunt resistor (R_{sh}). In an ideal scenario, the series resistor would have zero resistance (R_s=0), and the shunt resistor would have infinite resistance (R_{sh}=∞).

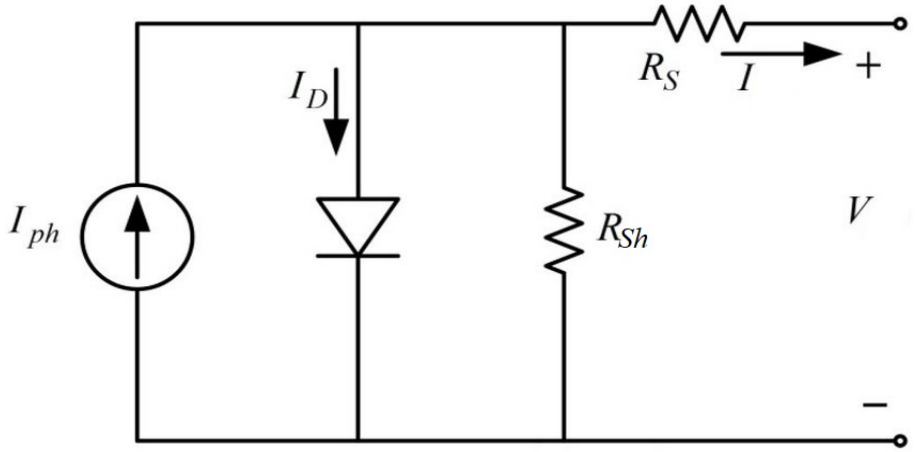

Figure 1.3: One diode equivalent circuit [4]

1.3.1 Ideal Photovoltaic Cell:

The basic equation that mathematically describes the I-V characteristic of the ideal photovoltaic cell is:

$$I = I_{\text{ph}} - I_{\text{d}} \tag{1.1}$$

where I_d is is given by the Shockley equation:

$$I_{\text{d}} = I_{0,\text{ cell}} \left[exp\left(\frac{qV}{aKT}\right) - 1 \right] \tag{1.2}$$

by replacing (1.2) in (1.1) we get:

$$I = I_{\text{ph}} - I_0 \left[exp\left(\frac{V + IR_{\text{s}}}{aV_t}\right) - 1 \right] \tag{1.3}$$

figure 1.4 shows the I-V curve originated from equation (1.3)

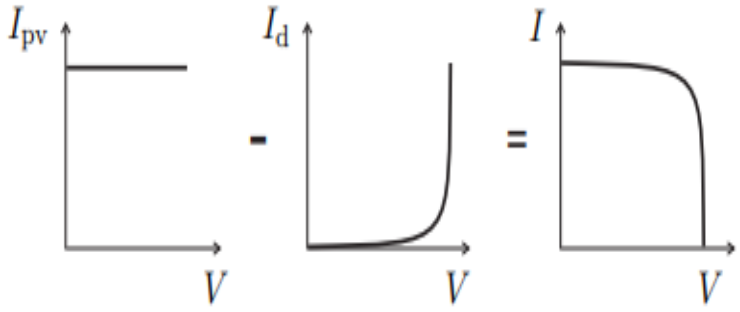

Figure 1.4: I-V characteristic of an ideal photovoltaic cell

1.3.2 Modeling of Photovoltaic Array:

The I-V characteristic equation (1.3) of a single photovoltaic cell does not accurately depict the behavior of a real-world photovoltaic array composed of multiple interconnected cells. To properly analyze the characteristics of the photovoltaic array, additional parameters must be added to the basic equation (1.3) as in [5].

$$I = I_{ph} - I_0 \left[exp\left(\frac{V + IR_{\text{s}}}{aV_t}\right) - 1 \right] - \frac{V + IR_{\text{s}}}{R_{\text{sh}}} \tag{1.4}$$

where: I: is the output current

I_{ph}:is the light generated current (it's directly proportional to the Sun irradiation) in (A),

I_0:is the reverse saturation or leakage current of the diode in (A),

V:is the output voltage,

R_{s}: is the series resistance,

R_{sh}: is the shunt resistance,

a: is the ideality factor

V_t: is the thermal voltage, with:

$$V_t = \frac{NsKT}{q}$$

If the array is composed of N_p parallel connections of cells the photovoltaic and saturation currents can be expressed as: $I_{pv} = I_{pv,cell}N_p, I_0 = I_{0,cell}N_p$.

1.4 I-V and P-V Characteristics of PV Device:

Equation (1.4) demonstrates that the output voltage and current of PV panels are not linearly related. Rather, their relationship is complex and non-linear, dependent on natural variables such as solar irradiation and ambient temperature that can vary over time.

1.4.1 I-V and P-V Characteristics of PV Cell:

Figure 1.5 shows I-V and P-V curves characteristic of the photovoltaic cell operating under standard test conditions.

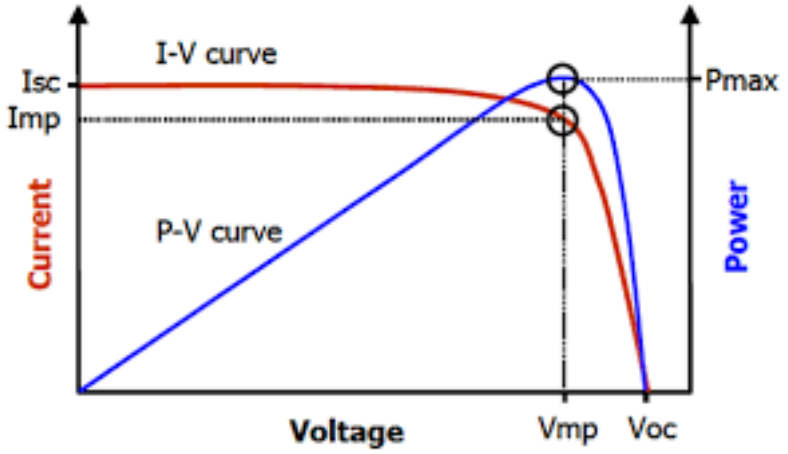

Figure 1.5: I-V and P-V curves characteristic of the photovoltaic cell [6]

The I-V curve represents the relationship between the electrical current flowing through the PV cell and the voltage applied across its terminals, while the P-V curve demonstrates the relationship between electrical power output and the voltage across its terminals.

The I-V and P-V curves show five critical points, which are essential for understanding the operating characteristics of PV cell, which are:

- **Open Circuit Voltage (V_{oc}):** is the maximum possible voltage that PV cell can generate when the current through it is 0 amp, no load condition (open circuited).
- **Short Circuit Current (I_{sc}):** is the highest possible current that a cell can generate when the voltage across its terminals equals 0V (short-circuited "R=0").
- **Maximum Power Point (MPP):** is the point at where the PV cell operates at maximum power output (P_{max}).
- **Current at Maximum Power Point (I_{mpp}):** represents the current produced by the PV cell when operating at the maximum power point. As shown in figure 1.5 its value is lower than the short circuit current (I_{sc}).
- **Voltage at Maximum Power Point (V_{mpp}):** represents the voltage produced by the PV cell when operating at the maximum power point. As shown in figure 1.5, its value is lower than the open voltage (V_{oc}).

In addition to these five critical point it is important to highlight the fill factor and efficiency:

- **Fill Factor (FF):**is the ratio of the maximum power (P_{max}) that the PV cell can produce to the product of the open circuit voltage (V_{oc}) and short circuit current (I_{sc}). In other words, it represents the ability of the PV cell to convert sunlight into electricity. A higher fill factor indicates a more efficient PV cell.

$$FF = \frac{Pmax}{Isc * Voc}$$

- **Efficiency (η):**is a measure of how effectively a photovoltaic cell converts sunlight into electrical energy. It is calculated by dividing the maximum output power (Pmax) by the input power (Pin) and is expressed as a percentage. This percentage represents the proportion of input sunlight power that is converted into electrical power. Since input power is measured in terms of power density, the efficiency can be determined by multiplying the power density at Standard Test Conditions (STC) by the area of the PV array [7].

$$\eta = \frac{Pmax}{Pin * Area}$$

1.4.2 I-V and P-V Characteristics of PV Module:

As previously mentioned, there are various ways to increase the output of a PV module, which are:

1.4.2.1 Series Combination of PV Cells:

If the cells are connected in series, the output voltage increases depending on the number of cells, whereas the current remains the same. (See figure 1.6)

1.4.2.2 Parallel Combination of PV Cells:

If the cells are connected in parallel, the output current increases depending on the number of cells, whereas the voltage remains the same. (See figure 1.6)

1.4.2.3 Series-Parallel Combination of PV Cells:

in this case, both current and voltage increases, hence the solar panels are made by using series-parallel combinations.

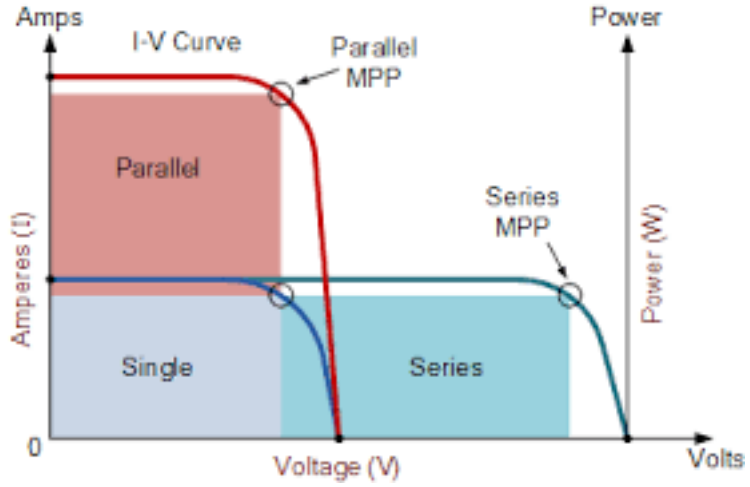

Figure 1.6: effect of cells connection on the I-V curve characteristic of the photovoltaic panel[8]

1.4.3 Irradiance and Temperature Effect on the I-V and P-V Characteristics:

The performance of a photovoltaic device depends on external factors such as solar radiation and temperature, which affect the current-voltage (I-V) characteristics seen in figure 1.7.

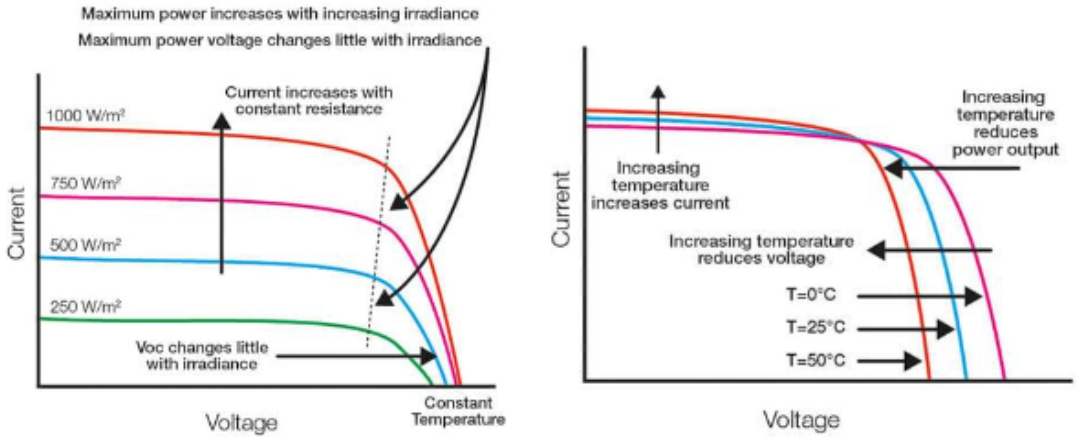

Figure 1.7: effect of irradiation and temperature change on the I-V curve characteristic of the PV panel [8].

Figures 1.7 illustrate that as temperature rises, the voltage of the PV device decreases while the current increases slightly. Conversely, with increasing irradiation, the current increases while the voltage slightly decreases. In addition, figure 1.8 demonstrates that the power output is directly proportional to the irradiance level and inversely proportional to the temperature. It also indicates that the maximum power point varies with changes in temperature and irradiation.

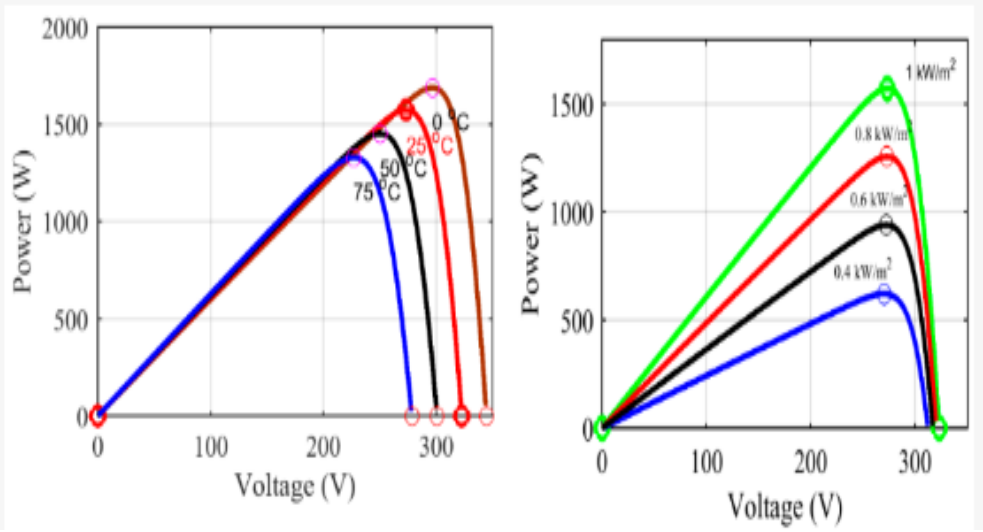

Figure 1.8: effect of irradiation and temperature change on the P-V curve characteristic of the photovoltaic panel [9].

Temperature and irradiance have a direct influence on the electrical characteristics of a photovoltaic module. To show this impact, specific equations are used:

- The light generated current of the photovoltaic cell depends linearly on the solar irradiation and is also influenced by the temperature according to the following equation[5]:

$$I_{\text{ph}} = (I_{\text{ph,n}} + K_i \Delta T)\frac{G}{Gn} \tag{1.5}$$

  where $I_{\text{ph,n}}$ is the light generated current at the nominal conditions (25°C and 1000W/m²) ΔT=T-T_n where T and T_n are the actual and nominal temperature in Kalvin respectively. G and G_n are the actual and nominal irradiation on the device in [W/m²] respectively.

- The diode saturation current I_0 and its dependence on the temperature may be expressed

by:

$$I_0 = I_{0,n}\left(\frac{T_n}{T}\right)^3 \exp\left(\frac{qE_g}{ak}\left(\frac{1}{T_n}-\frac{1}{T}\right)\right) \tag{1.6}$$

Where Eg is the bandgap energy of the semiconductor (Eg≈1.12eV),and $I_{0,n}$ is the nominal saturation current:

$$I_{0,n} = \frac{I_{\text{sc,n}}}{\exp\left(\frac{V_{\text{oc,n}}}{aV_{\text{t,n}}}\right)-1} \tag{1.7}$$

1.5 Maximum Power Point (MPP):

The maximum power of solar panels corresponds to a single operating point called the maximum power point (MPP). This point depends mainly on the irradiance, the temperature and the variations of the load which are variable with time. The output voltage and current of the photovoltaic modules results in the maximum power output. In most photovoltaic power systems, a particular control algorithm, namely, maximum power point tracking (MPPT) is utilized to take full advantage of the available solar energy. The operation of maximum power point tracking is to adjust the power interfaces so that the operating characteristics of the load and the photovoltaic array match to ensure the transfer of the maximum power [10].

1.6 History of Maximum Power Point Tracking:

When a PV module is directly coupled to a resistive load or to a dynamic load (e.g. DCmotor) the module output current (I) and voltage (V) depend on the module's operating point. The module's operating point is located at the intersection of module and load I-V curve. Unfortunately, the module I-V curve is non-linear with only one maximum power point (MPP) at which the intersection rarely occurs. Also, the module I-V and P-V curves change under varying irradiation and ambient temperature conditions making the new location of the MPP as shown in figure 1.9.When the module is partially shaded , the P-V curve has multi-peaks as shown in figure 1.7. Starting in 1954, the maximum power point tracking (MPPT) is the aim of researchers to enhance the efficiency and improve the performance of P-V systems [11].

In 1985, Australian Energy Research Laboratories (AERL) was founded by Stuart Watkinson

(BE Elec. Eng., Grad. M.I.E.A) , in that laboratories a “Power Optimizer” was developed , a revolutionary solution to a complex problem. The “Power Optimizer” would be known as the AERL MAXIMIZER, the world’s first truly Universal Maximum Power Point Tracker (MPPT) [12].

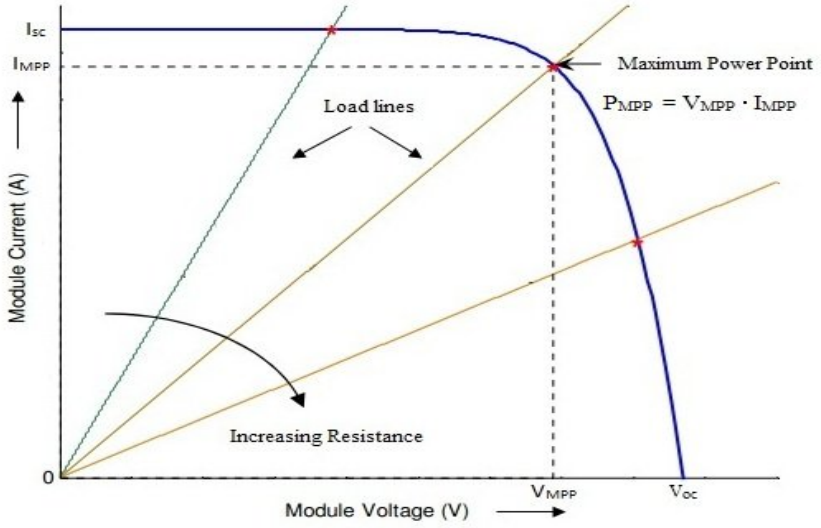

Figure 1.9: Location of operating point as influenced by resistive load (R)

1.7 MPPT Techniques:

Electrical MPPT techniques are classified into families:

1. **OFF-Line Techniques :** such as fractional open-circuit voltage (FOCV) and fractional short-circuit current (FSCC) techniques.

2. **ON-Line or Hill-Climbing(HC):**such as perturb and observe (P&O)and incremental conductance (InCond) techniques

3. **Artificial Intelligence (AI) Techniques:** for example fuzzy logic control (FLC) technique, artificial neural network (ANN) technique ,particle swarm optimization (PSO) technique and genetic algorithm as shown in figure 1.11 [13].

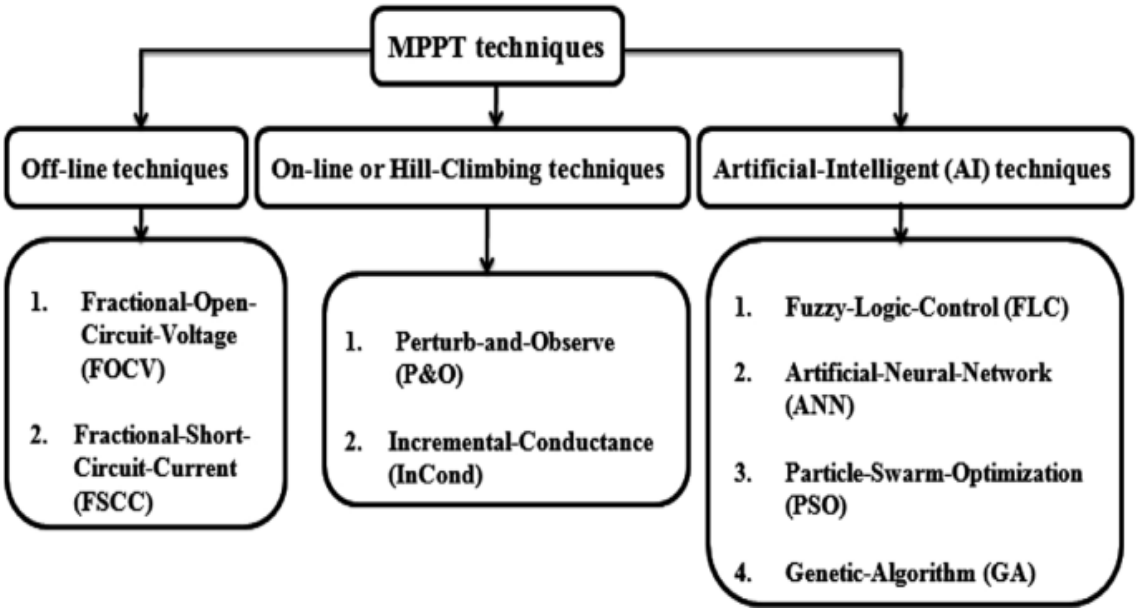

Figure 1.10: MPPT techniques

These MPPT techniques fail or deviate from tracking the correct maximum power point (MPP) under sudden change of solar irradiance and ambient temperature as well as under partial shading which can affect the steady state performance by causing oscillations around the MPP therefore the system would have more losses .

1.8 DC-DC Converter:

The main component of an MPPT system is a DC-DC converter that connects the load and the module and is responsible for delivering the maximum amount of power from the PV module to the load. The load impedance as seen by the source (Rin) is adjusted and matched at the point of maximum power with the source by varying the duty cycle (D), which allows the source to transfer the most power.

There are several topologies available for DC-DC converter :

1.8.1 Boost Converter:

Step up the DC input voltage. Figure 1.11 shows the diagram of the boost converter , when the power switch is ON , the inductor charge energy in the form of electromagnetic field

and discharge energy when power switch is OFF. The capacitor reduces the voltage ripple . The output voltage depends on the duty ratio of the switch and the applied input voltage, which is defined as:

$$V_{OUT} = V_{IN}(1 - D) \tag{1.8}$$

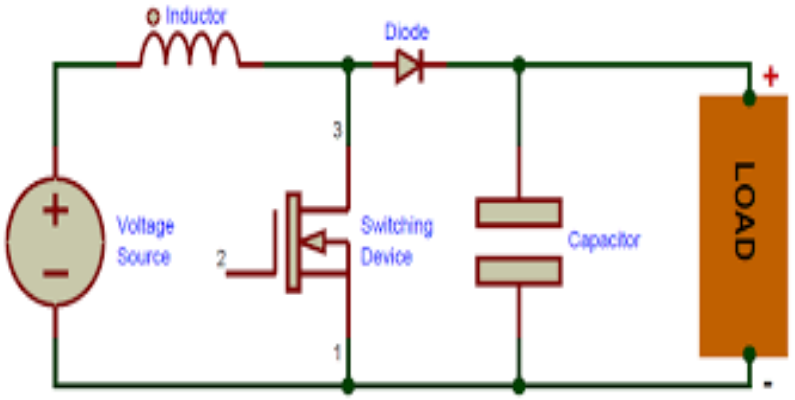

Figure 1.11: Circuit diagram of boost converter

1.8.2 Buck Converter:

Where the output voltage is less than the applied input voltage.More detailed explanation is provided in chapter 2.

$$V_{OUT} = V_{IN}D \tag{1.9}$$

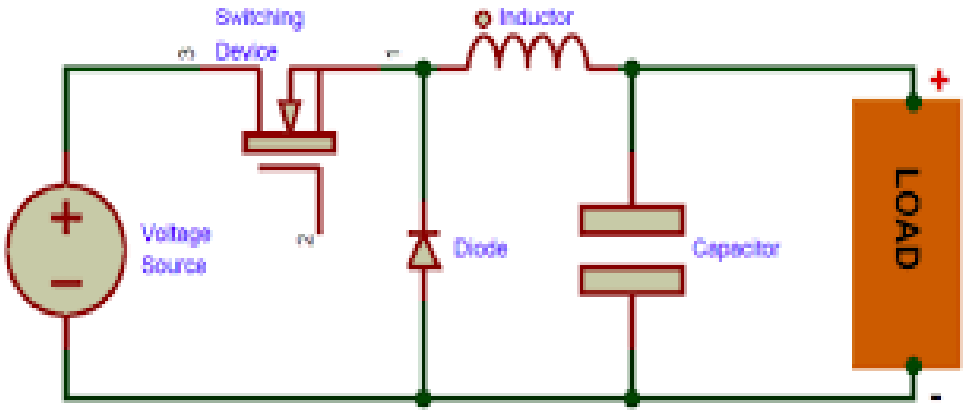

Figure 1.12: Circuit diagram of boost converter

1.8.3 Buck-Boost Converter:

This converter is used to do both ,increase or decrease the voltage level of the applied input voltage. Circuit diagram of buck - boost converter is shown in figure 1.13, the output voltage equation can be defined as

$$V_{OUT} = \frac{D}{(1-D)V_{IN}} \tag{1.10}$$

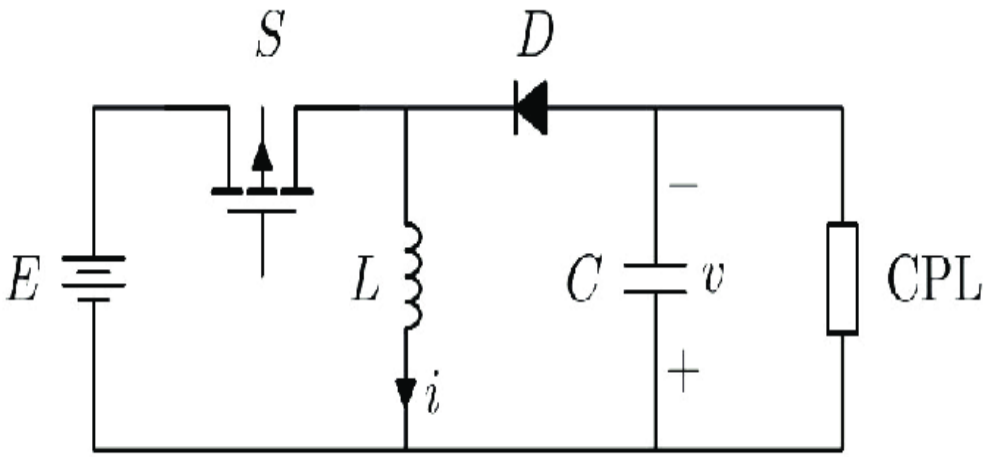

Figure 1.13: Circuit diagram of buck-boost converter

1.9 Conclusion:

This chapter provided an overview of photovoltaic technology and focused on the PV modeling, specifically the I-V and P-V characteristics. It also included a brief history of Maximum Power Point Tracking (MPPT) and highlighted various techniques used for power extraction, as well as different DC-DC converters used in PV systems. The designing and sizing methods and algorithms used in controlling are presented in the next chapter.

Chapter 2

Analysis and design of The MPPT System

2.1 Introduction:

Photovoltaic modules are just one component of the overall photovoltaic system; they produce a voltage that needs to be converted from one level to another using a DC-DC buck converter in a regulated manner using MPPT algorithms to extract the maximum power out of them and maintain a constant output DC voltage . In this chapter the design and sizing of the DC-DC converter are discussed;the storage element is described;the sizing and design of the driver bootstrap circuit used to bias the MOSFET is explained ;and the different MPPT techniques are presented.

2.2 Standalone PV System:

Many photovoltaic systems operate in a stand-alone mode. Such systems consist of a PV generator, energy storage (for example a battery), AC and DC loads ,elements for power conditioning and a damping load – as shown in figure 2.1. Per definition, a stand-alone system involves no interaction with a utility grid. A PV generator can contain several arrays. Each array is composed of several modules, while each module is composed of several solar cells. The battery bank stores energy when the power supplied by the PV modules exceeds load demand and releases it backs when the PV supply is insufficient. The load for a stand-alone PV system can be of many types, both DC (television, lighting) and AC (electric motors, heaters, etc.). The power conditioning system provides an interface between all the elements of the PV system, giving protection and control. The most frequently encountered elements of the power conditioning system are blocking diodes, charge regulators and DC-AC converters[14]. In addition, the damping load is needed for damping the excess energy which is produced in case of the energy generated by PV array is more than the load demand and the storage batteries are fully charged, simultaneously [15].

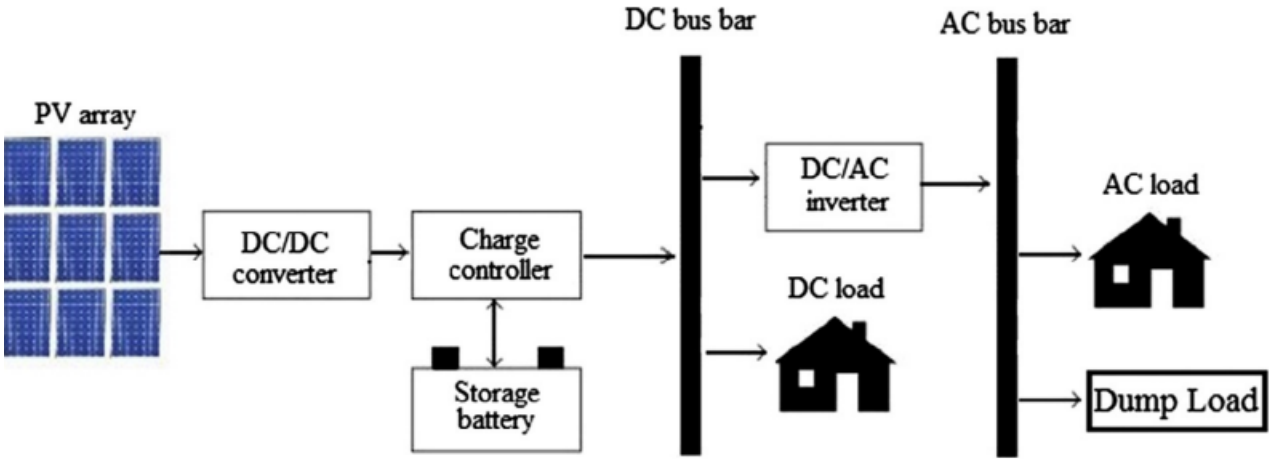

Figure 2.1: A typical basic components of a standalone PV system[15]

2.3 Pulse Width Modulation:

Switching power converters are used in modern DC-DC converters to convert and deliver energy to any load. Pulse Width Modulated (PWM) signals are used to control switches in those converters. PWM signals are pulses with fixed frequency and magnitude and variable pulse width. The width of the pulses changes from pulse to pulse according to the duty cycle. When a PWM signal is applied to the gate of a power transistor, it causes the turn-ON and turn-OFF intervals of the transistor to change from one PWM period to another . The frequency of a PWM signal must be much higher than that of the modulating signal, such that the energy delivered to the load depends mostly on the PWM signal During the operation of the converter, the switch will be switched at a constant frequency $f_S$with an ON-time of DTs, and an OFF-time of (1 - D)T_s, where T_s is the switching period $T_s = \frac{1}{f_s}$ and D is the duty cycle of the switch (D ϵ [0, 1]) : $D = \frac{T_{ON}}{T_{ON}+T_{0FF}}$ [16].

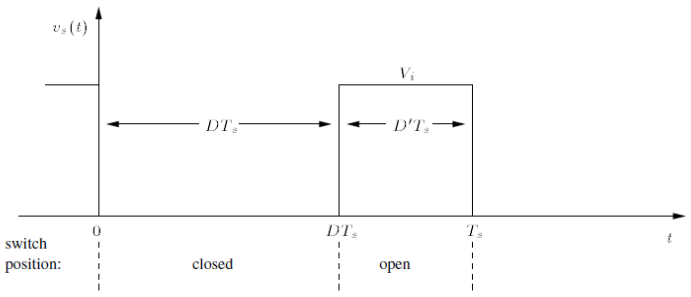

Figure 2.2: Pulse width modulation waveform

2.4 DC-DC Converters:

In this section the principles of switching power conversion are introduced and details of buck converter circuit are discussed. The mathematical model for the buck is derived to represent the circuit's steady-state and dynamic behaviors. The converter presented is a switching converter consists of capacitors, inductor, diodes and switch. All these devices ideally do not consume any power, which is the reason for the high efficiency of switching converters. The switch is a semiconductor device ,the one used is the MOSFET(Metal Oxide Semiconductor Field Effect Transistor), it has a low power consumption ,high switching speed and it can handle a high voltage and current levels

2.4.1 Modes of Operation in Buck Converter:

There are two modes of operation in buck converter :

1. **Continuous Conduction Mode(CCM):** The converter is said to be operating in a continuous conduction mode if the load current never becomes zero during the complete cycle. To understand its origin,the inductor current ripples equation will be examined [17].
   -The inductor ripples ΔI_L is:

$$\Delta I_L = \frac{(V_{in} - V_{out})}{2L} DT_s \tag{2.1}$$

   It can be seen from the inductor ripple equation that the value of inductor's current ripples is inversely proportional to the inductance. If the inductance value is reduced, then the ripple will increase. Furthermore,reducing the inductance value will increase the ripples such that ripples will become more than the load current. At that time, the operation of converter will change from CCM to DCM because the load current will become zero for some instant.as shown in figure2.3 [18]. If the load resistance is increased then the load current will decrease and the graphs in figure 2.3 will become as shown in figure2.4.

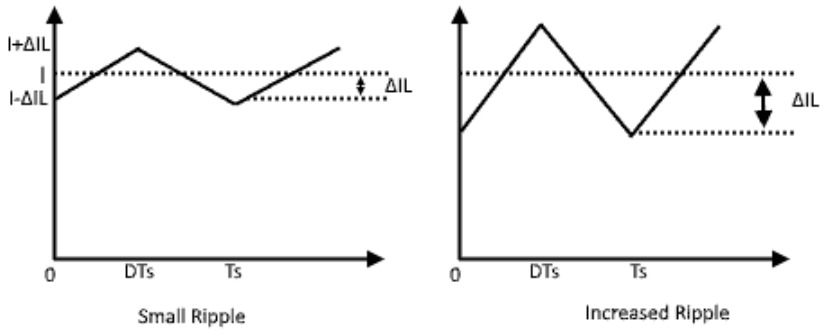

Figure 2.3: current ripple

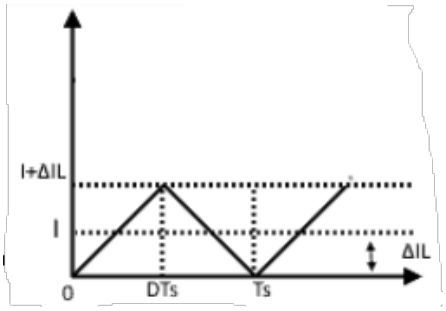

Figure 2.4: reduced load current

The graph above also demonstrates the critical boundaries between CCM and DCM where further increasing in the load resistance or increasing the current ripple will change the operation from CCM to DCM [17].

2. **Dis-continuous Conduction Mode (DCM) :**Where the Inductor current remains zero for some time in the switching period because the inductor current ripples are more than the load current. Therefore, during OFF time, the load current starts decreasing till it becomeS zero as shown in figure 2.5 [17].

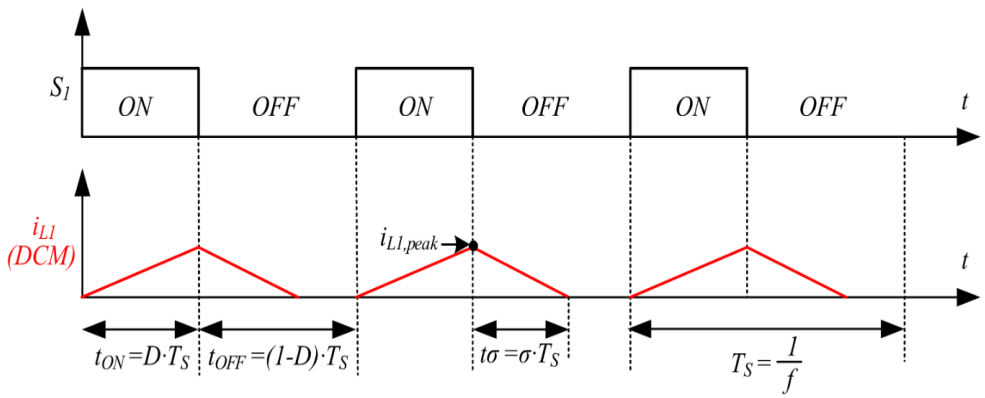

Figure 2.5: dis-continuous conduction mode in buck converter waveform

2.4.2 Transfer Function of Buck Converter:

To derive the transfer function of the converter;it needs to be considered in steady state . The average voltage across the inductor is zero in steady state according to volt second balance. Furthermore, the inductor will act as a short circuit in steady state to a pure DC [19].

$$< V_L >= V_{LON}t_{ON} + V_{LOFF}t_{OFF} = 0 \tag{2.2}$$

i) When the switch is ON(MOSFET) the inductor will be charged and the voltage accross it is:

$$V_{LON} = V_{IN} - V_{OUT} \tag{2.3}$$

$$t_{ON} = DT_s \tag{2.4}$$

ii) When the switch is OFF the diode will be forward bias and it will strat conducting , the inductor discharged causing its voltage to reverse polarity . The voltage across it will be :

$$V_{LOFF} = -V_{OUT} \tag{2.5}$$

$$t_{OFF} = T_S – t_{ON} = T_s – DT_S = (1 - D)T_S \tag{2.6}$$

Replacing in the equation (2.2) :

$$< V_L >= (V_{IN} – V_{OUT})DT_S + (–V_{OUT})(1–D)T_S = 0$$

$$V_{IN}D – V_{OUT}D – V_{OUT} + V_{OUT}D = 0$$

The final form of the transfer function is:

$$V_{OUT} = DV_{IN} \tag{2.7}$$

2.4.3 Inductor Current :

Minimum inductor current I_{LMIN} and maximum inductor current I_{LMAX} are both most important terms in designing. Therefore, both minimum peak and maximum peak of the current need to be found. Understanding more how the buck-converter works simplifies the derivation of both variables ;therefore the detailed derivation will be described in the upcoming sections.
i) By turning ON the MOSFET . The inductor current is :

$$I_L = I_{IN} \tag{2.8}$$

The inductor will charge during turn ON time. This current further divide into load current I_{OUT} and capacitor current I_C.

$$I_L = I_C + I_{LOAD} \tag{2.9}$$

The inductor voltage V_{LON} during this period is the voltage difference between applied DC input voltage $V_{IN}$and output voltage V_{OUT}

$$V_{LON} = V_{IN} - V_{OUT} \tag{2.10}$$

The average voltage across inductor V_L is zero according to volt second balance. Recalling the duty cycle equation, the turn ON time (t_{ON}) is the product of duty cycle D and total period T_S.

$$t_{ON} = DT_s \tag{2.11}$$

The rippling current during turn-ON mode can be found from inductor current voltage relationship:

$$V_L = L\frac{di}{dt}$$

$$\frac{di}{dt} = \frac{V_L}{L}$$

By replacing with the equation of V_L we get:

$$\frac{di}{dt} = \frac{V_{IN} - V_{OUT}}{L}$$

$$\Delta I_{LON} = \Delta t_{ON} \frac{V_{IN} - V_{OUT}}{L}$$

By putting the value of Δt_{ON}, the final form of the equation is given as:

$$\Delta I_{LON} = DT_S \frac{(V_{IN} - V_{OUT})}{L} \tag{2.12}$$

Figure2.6 demonstrates the rippling current that first increases in the ON time and then decreases in the OFF time and also shows the voltage across the inductor

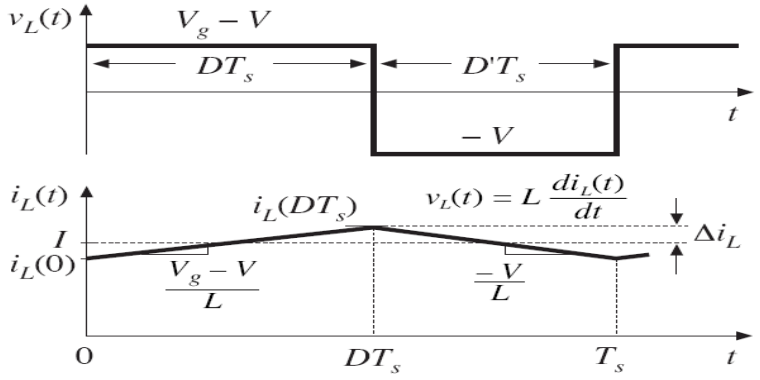

Figure 2.6: inductor's current and voltage waveforms

2.4.4 Components Design and Ratings for Buck Converter:

This section will discuss the designing of components used in buck converter with their ratings.

2.4.4.1 Inductor Sizing:

This section will describe the important aspect of inductor required for buck converter. This includes two main ideas which are the critical inductance and peak current rating of inductor.

1. **Critical Inductance** L_C **:**Is Minimum Inductance value at which the inductor current

reaches Boundary Conduction Mode, I_{LMIN} is used to determine the Critical Inductance. Any inductance lower than critical inductance will cause the buck to operate in Discontinuous Conduction Mode.

The requirement is set by max ΔI_L discussed previously. For operating buck converter in CCM mode.

I_{LMIN} can be determined :

$$I_{LMIN} = I_L - \frac{\Delta iL}{2} = \frac{V_{OUT}}{R} - \frac{1}{2}\left(\frac{V_{OUT}}{L}(1-D)T_S\right)$$

$$I_{LMIN} = V_{OUT}\left(\frac{1}{R} - \frac{(1-D)}{2Lf_S}\right) \tag{2.13}$$

To obtain the equation of the critical inductance we set :

$$I_{LMIN} = 0$$

$$I_{LMIN} = V_{OUT}\left[\frac{1}{R_{MAX}} - \frac{(1-D_{MAX}}{2L_C f_s}\right]$$

$$L_C = \frac{(1-D_{MAX})R_{MAX}}{2f_S} \tag{2.14}$$

- $D_{MAX}$is calculated input voltage for L_C.
- $R_{MAX}$is calculated at minimum output current.

$$I_{OUT(MAX)} = \frac{P_{OUT(PEAK)}}{V_{OUT(MIN)}} \tag{2.15}$$

$$I_{OUT(MIN)} = 10\% I_{OUT(MAX)} \tag{2.16}$$

$$R_{MAX} = \frac{V_{OUT(MAX)}}{I_{OUT(MIN)}} \tag{2.17}$$

The inductor value is chosen more than critical inductance:

• L $< L_C$ for operating buck converter in DCM

• L $>10L_C$ for operating buck converter in CCM [19].

2. **Peak Current Rating of Inductor:** The peak current rating of inductor can be found using maximum value of the inductive current I_{LMAX}. The maximum inductor current occurs at maximum load. The peak current rating of inductor can be found using the equation of maximum inductor current as given as [18]:

$$I_{LMAX} = I_L + \frac{\Delta iL}{2} = \frac{V_{OUT}}{R} + \frac{1}{2}\left(\frac{V_{OUT}}{L}(1-D)T_S\right)$$

$$I_{LMAX} = V_{OUT}\left[\frac{1}{R_{MIN}} - \frac{(1-D_{MIN})}{2Lf_S}\right] \tag{2.18}$$

- D_{MAX} is calculated from highest input voltage.
- The value of L must be chosen as discussed previously.

2.4.4.2 Output Capacitor Sizing:

The capacitor is designed such that the required function is performed in a safe mode and it serves as a filter by providing a path for the harmonic currents away from the load [20].

1. **Voltage Rating:**The capacitor is specifically designed and selected to ensure that it can endure the maximum output voltage. Ideally, the capacitor's maximum voltageV_{CMAX} is given below:

$$V_{CMAX} = V_{OUT} + \frac{\Delta V_{OUT}}{2} \tag{2.19}$$

$\Delta\, V_{OUT}$ is the output ripple voltage.

For practical capacitors the case is different. Practical capacitor disturbs the term $\frac{\Delta V_{OUT}}{2}$because practical capacitors have ESR (equivalent series resistance). The contribution shown by ESR for output voltage ripple is (ESR * ΔI_L). This contribution made by ESR can be suppressed by using following methods[17]:

(a) By Reducing ESR: Reducing the ESR will reduce the voltage ripple disturbance. The ESR can be reduced by means of two methods. Either by connecting capacitors

in parallel or by using capacitors that have low value of ESR.

(b) Reduce $\Delta I_L$by increasing the switching frequency or choosing bigger value of inductor L.

2. **Minimum Capacitance According to Voltage:**The AC component (ripple) of inductor current flows through the capacitor, leaving the average current flowing through the load(battery).The waveform of the capacitor current is shown in figure2.7.

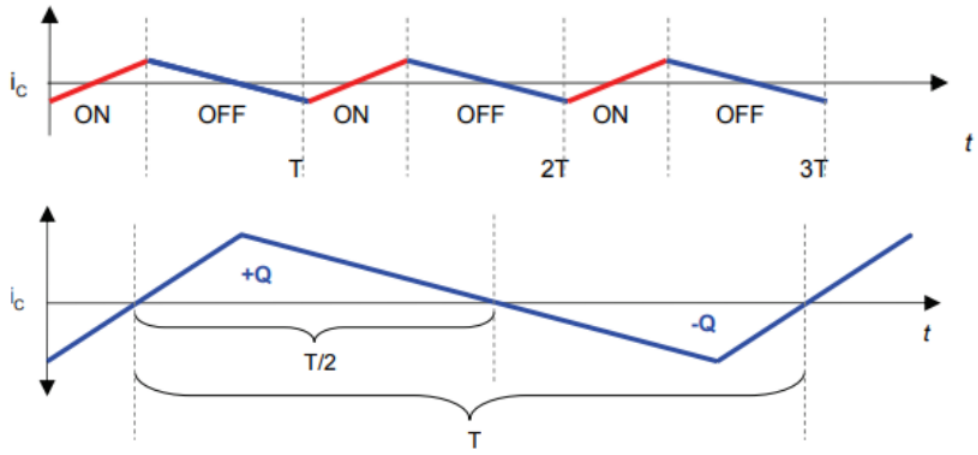

Figure 2.7: output capacitor current waveform

It can be seen form figure2.7 that the charge is the product of area and slop

$$Q = area.\Delta = \frac{1}{2}\left(\frac{T}{2}\right)\left(\frac{\Delta I_L}{2}\right) = \frac{\Delta I_L}{8f_s} = \frac{\frac{V_{OUT}}{L}(1-D)T_s}{8f_s} = \frac{(1-D)V_{OUT}}{8Lf_s^2} \quad (2.20)$$

As we know:

$$Q = C.\Delta V_{OUT} \Rightarrow C = \frac{Q}{\Delta V_{OUT}} \quad (2.21)$$

We replace (2.20) in (2.21) we get :

$$C = \frac{(1-D)V_{OUT}}{8Lf_s^2\Delta V_{out}} = \frac{(1-D)}{8Lf_s^2\left(\frac{\Delta V_{OUT}}{V_{OUT}}\right)}$$

The final expression for finding the suitable output capacitance is :

$$C_{OUT} = \frac{(1 - D_{MIN})}{8Lf_s^2 \left(\frac{\Delta V_{OUT}}{V_{OUT}}\right)} \tag{2.22}$$

$\left(\frac{\Delta V_{OUT}}{V_{OUT}}\right)$ is the peak to peak value of output voltage ripple percentage.

- A commonly accepted output voltage ripple is to keep it below 5%of the average output voltage[20].

3. **RMS Current Rating:** the RMS current rating equation can be found as:

$$I_C = I_{LMAX} - I_{OUT} = I_{OUT} + \frac{\Delta I_L}{2} - I_{OUT} = \frac{\Delta I_L}{2} \tag{2.23}$$

$$I_{Crms} = \frac{I_C}{\sqrt{3}} = \frac{\frac{\Delta I_L}{2}}{\sqrt{3}}$$

$$I_{Crms} = \frac{(1 - D_{MIN})V_{OUT}}{2\sqrt{3}Lf_s} \tag{2.24}$$

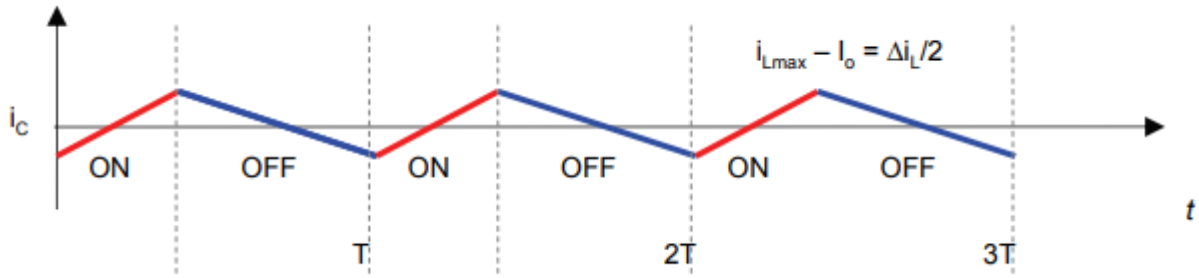

Figure 2.8: output capacitor RMS current waveform

2.4.4.3 Input Capacitor Sizing:

1. **Voltage Rating:** Capacitor Voltage should withstand the maximum input voltage

   – Ideally: $V_{CMAX} = V_{INMAX}$

   – More realistic: Capacitor has ESR (Equivalent Series Resistance) contributes to capacitor loss

– By reducing ESR ,the loss contribution is minimized [19].

2. **Minimum Capacitance According to Current:**The input capacitor is chosen in a way to minimize ripples in the input voltage, as too much of a ripple is actually harmful to the energy harvesting system, particularly when the power recovered curve versus input voltage P(V_{IN}) is quite at the localized maximum.Which is particularly the case with powerful solar panels[20].

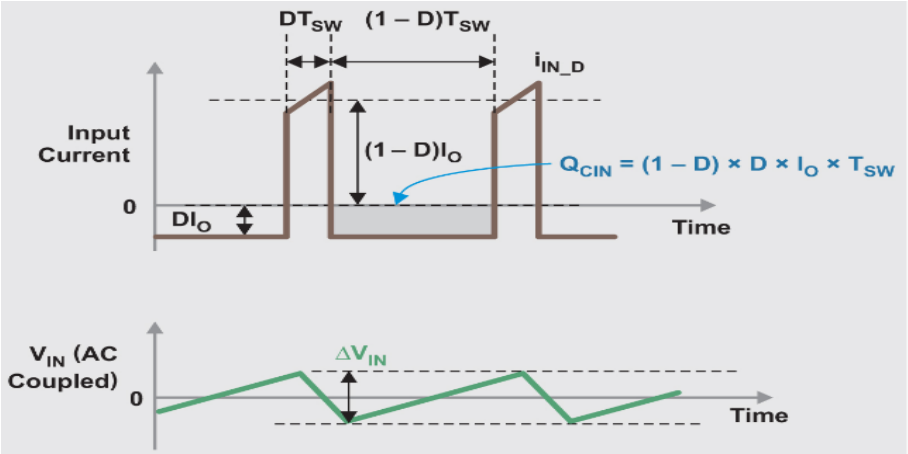

Figure 2.9: input capacitor current waveform .

From the figure 2.9, the charge is the area of the OFF region

$$Q = area(OFF) = t_{OFF} DI_{OUT} = (1-D)TDI_{OUT} = \frac{(1-D)DI_{OUT}}{f_S} \tag{2.25}$$

The capacitance is the charge divided by the voltage therefore:

$$C_{IN} = \frac{Q}{\Delta V_{IN}} = \frac{\frac{(1-D)DI_{OUT}}{f_S}}{\Delta V_{IN}}$$

$$C_{IN} = \frac{(1-D)DI_{OUT(MAX)}}{\Delta V_{IN} f_s} \tag{2.26}$$

2.4.4.4 Switch Design:

1. **Current Rating:**The waveforms of the switch current , diode and inductor current are shown below for turn ON and turn OFF time.

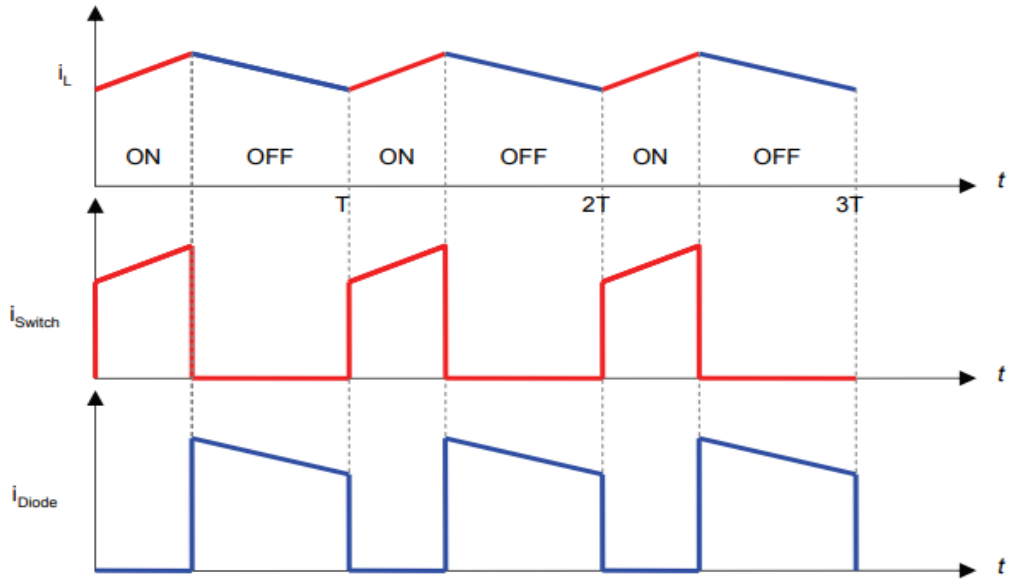

Figure 2.10: current waveforms for inductor,switch and diode

The average switch current I_{switch} is:

$$I_{Switch} = \frac{(i_{Lmax} + i_{Lmin})T_{ON}}{2T_s}$$

$$I_{Switch} = \frac{[i_{Lmax} + (i_{Lmax} - \Delta i_L)]DT_S}{2T_S} = \frac{(2i_{Lmax} - \Delta i_L)D}{2}$$

$$I_{Switch} = \left(i_{Lmax} - \frac{\Delta i_L}{2}\right) D = I_L D = I_{OUT} D$$

Therefore the final form of the equation of current rating for the switch become:

$$I_{Switch} > I_{OUT} D \tag{2.27}$$

2. **Voltage Rating:**For ideal diode, the $V_{SWITCH(MAX)}$ is equal to$V_{IN(MAX)}$ while for non-ideal diode; $V_{SWITCH(MAX)}$ is equal to $V_{IN(MAX)}$plus V_F. the additional term V_F is the maximum diode forward voltage drop For ideal diode[18].

- $V_{SWITCH(MAX)}$= $V_{IN(MAX)}$
- For non-ideal diode $V_{SWITCH(MAX)}$ = $V_{IN(MAX)}$ +V_F
- Safety factor of 20% is used.

2.4.4.5 Diode Design:

1. **Current Rating:**The same approach is adopted for calculating current rating for diode as it was adopted for the calculation of the switch. The average forward diode current is calculated from the current waveform of the diode. As diode conduct during off time of the switch therefore, t_{OFF} is considered in the calculation[19]:

$$I_{DIODE} = \frac{(i_{Lmin} + i_{Lmax})T_{OFF}}{2T_S}$$

$$I_{DIODE} = \frac{((i_{Lmax} - \Delta i_L) + i_{Lmax})\,(1-D)T_S}{2T_S} = \frac{(2i_{Lmax} - \Delta i_L)(1-D)}{2} = I_L(1-D)$$

$$I_{DIODE} = I_{OUT}(1-D)$$

Therefore the final form of the equation of current rating for the switch become:

$$I_{DIODE} > I_{OUT}(1 - D_{MIN}) \tag{2.28}$$

2. **Voltage Rating:** V_{PRM} or PIV (peak inverse voltage) is the maximum voltage across the diode. It is given in the data sheet of the component. For ideal switch, peak inverse voltage V_{PRM} is equal to maximum input voltage $V_{IN(MAX)}$. For non-ideal case, V_{PRM} is equal to $V_{IN(MAX)}$ plus maximum forward voltage drop V_{SWITCH}across the switch[18].

$$V_{PRM} = V_{IN(MAX)} + V_{SWITCH} \tag{2.29}$$

Where, the value of V_{SWITCH} is the maximum forward voltage drop across the switch . For this calculation, it will allow the safety factor at least greater than 20%.

2.5 Storage Element :

PV stand alone or hybrid power generation systems has to store the electrical energy in batteries during sunshine hours to provide continuous power to the load under varying environmental conditions .

2.5.1 Lead Acid Battery:

Battery is an energy storage device that consists of one or more of electrochemical cells that transform stored chemical energy into electrical energy;batteries of PV systems are subjected to frequent charging and discharging process. Lead acid batteries are the common energy storage devices for PV systems. Lead acid batteries can be either 6V or 12V type ,in a solid plastic container. The batteries can be flooded cell type or sealed/gel type. The life time of the batteries varies from 3 to 5 years[21].

The batteries for PV applications are to be designed to meet the following characteristics: [22]

1. Low cost
2. High energy efficiency
3. Low maintenance
4. Good reliability and less self discharge
5. Wide operating temperature

Batteries are generally classified into primary and secondary batteries.

Primary batteries are disposable batteries. They are built to be used only once and then discarded or recycled, this is because the chemical reactions that take place within primary batteries cannot be reversed, and the active materials do not go back to their original forms.

Secondary batteries, also called rechargeable batteries, are built to be recharged and reused many times. They usually include active materials that are assembled in a discharged state. These batteries can be recharged upon the application of electric current, which helps to reverse the chemical reactions that take place when the battery is used. Secondary batteries are of significant interest for their ability to store and supply energy[23].

2.5.2 Battery Parameters:

1. **Battery Capacity:**The storage capacity of the battery is represented in Ampere-hour or Ah. If V is the battery voltage then the energy storage capacity of the battery can be Ah x V = Watt-hour. Usually battery capacity will be specified for a given discharge/charge rating or C rating. The actual capacity depends on operating conditions such as load, temperature, etc [21].

2. **Battery Voltage:** The terminal voltage during operating condition is known as nominal voltage or working voltage. This voltage will be specified by manufactures. It may be 3V, 6V, 12V, 24V etc [21].

3. **State Of Charge (SOC):** Is a measurement of the amount of energy available in a battery at a specific point in time expressed as a percentage (0% = empty, 100%=full)[21].

4. **Depth Of Discharge (DOD):** It gives a measure of energy withdrawn from a battery as percentage of its full capacity. The state of charge of a battery is the difference between the full charge and the depth of discharge of the battery in percentage. If the DOD is 25% then the state of charge is
(100 - 25) = 75% [21].

5. **Battery Life Cycle:** it is the number of complete charge – discharge cycles a battery can work before the nominal capacity decreases less than 80% of its rated initial capacity. After the specified life cycle, the battery will work with reduced capacity. It can be used but the capacity will be lower [21].

6. **Discharge/Charge Rate or C – Rate:** C-rating is the value obtained by giving the ratio of the capacity of the battery to the number of hours for full charge or discharge represented as $\frac{C}{X}$, where X is the time in hours for full charge or discharge. If X = 10 h then C-rating is $\frac{C}{10}$or 0.1C.
The charge or discharge current for a C- rating can be calculated by dividing Ah capacity by the total hours of charge and discharge. For a 50Ah capacity battery if C rating is 0.1 C then the charge or discharge current will be $\frac{50}{10} = 5A$ [21].

7. **Self Discharge:** it is the electrical capacity lost when a battery is not being used due to internal electrochemical process with the battery.The self discharge increases with the increase of temperature. The batteries can be stored at lower temperatures to reduce self discharge [21].

2.6 Bootstrap Circuit :

Driving MOSFET in half-bridge configurations present many challenges . One of those challenges is generating bias for the high-side MOSFET. A bootstrap circuit present a solution for this issue when it is properly designed.

2.6.1 Operation of Bootstrap Circuit:

The V_{BS}voltage (the voltage difference between the V_b and V_s pins on the control integrated circuit(IC)) provides the supply to the high side driver circuitry of the control IC's. This supply needs to be in the range of 10- 20V to ensure that the Control IC can fully enhance the MOS Gated Transistor (high side MOSFET) being driven, some of International Rectifier's Control IC's include undervoltage detection circuits for V_{bs}, to ensure that the IC does not drive the MOSFET if the V_{bs}voltage drops below a certain voltage (V_{bsuv} in the datasheet). This prevents the MOSFET from operating in a high dissipation mode.

This V_{bs}supply voltage is a floating supply that sits on top of the V_S voltage (which in most cases will be a high frequency square wave). There are a number of ways in which the V_{bs} floating supply can be generated, one of these being the bootstrap method described in this section. This method has the advantage of being simple and inexpensive but has some limitations. The duty cycle and ON-time are limited by the requirement to refresh the charge in the bootstrap capacitor . The bootstrap supply is formed by a diode and capacitor combination as shown in figure 2.11).

The operation of the circuit is as follows. When Vs is pulled down to ground (either through the low side MOSFET or the load, depending on the circuit configuration), the bootstrap capacitor (C_{bs}) charges through the bootstrap diode (D_{bs}) from the 12V V_{cc}supply. Thus providing a

supply to V_{bs} [24].

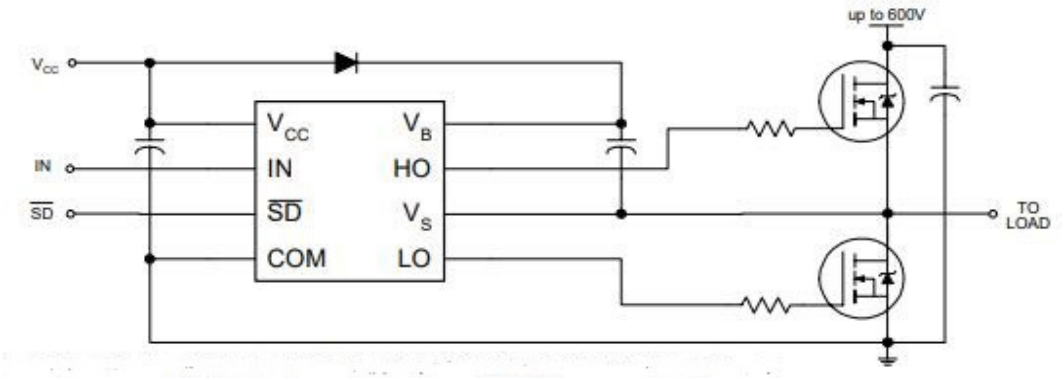

Figure 2.11: bootstrap circuit

2.6.2 Factors Affecting the Bootstrap Circuit:

There are five influencing factors which contribute to the supply requirement from the V_{bs} capacitor. These are:

1. The required gate charge
2. I_{qbs} - quiescent current for the high side driver circuitry
3. Currents within the level shifter of the control IC
4. MOSFET gate-source forward leakage current
5. Bootstrap capacitor leakage current

Factor 5 is only relevant if the bootstrap capacitor is an electrolytic capacitor, and can be ignored if other types of capacitor are used. Therefore it is always better to use a non-electrolytic capacitor if possible[25].

2.6.3 Bootstrap Capacitor C_{bs}:

The following equation details the minimum charge which needs to be supplied by the bootstrap capacitor[24]:

$$Q_{bs} = 2Q_g + \frac{I_{qbs(max)}}{f_S} + Q_{ls} + \frac{I_{cbs(leak)}}{f_s} \tag{2.30}$$

- Q_g:Gate charge of the MOSFET
- $I_{cbs(leak)}$:Bootstrap capacitor leakage current
- f_S:the switching frequency
- Q_{ls}:level shift charge required per cycle = 5nC (500V/600V IC's) or 20nC (1200V IC's)

The bootstrap capacitor must be able to supply this charge, and retain its full voltage, otherwise there will be a significant amount of ripple on V_{bs}, which could fall below the V_{bsuv} undervoltage lockout, and cause the HO output to stop functioning. Therefore the charge in the capacitor must be a minimum of twice the above value. The minimum capacitor value can be calculated from the equation below[24]:

$$C_{bs} = \frac{2Q_{bs}}{V_{cc} - V_F - V_{LS} - V_{min}} = \frac{2\left(2Q_g + \frac{I_{qbs(max)}}{f_S} + Q_{ls} + \frac{I_{cbs(leak)}}{f_s}\right)}{V_{cc} - V_F - V_{LS} - V_{min}} \tag{2.31}$$

- V_F:Forward voltage drop across the bootstrap diode
- V_{LS}:Voltage drop across the low side MOSFET (or load for a high side driver)
- V_{min}:Minimum voltage between V_B and V_S

-The C_{bs} Capacitor value obtained from the above is the absolute minimum required, however due to the nature of the bootstrap circuit operation, a low value capacitor can lead to over-charging, which could in turn damage the IC. Therefore to minimize the risk of overcharging and further reduce ripple on the V_{bs} the C_{bs} value obtained from the above equation should be multiplied by a factor of 15 .

2.6.4 Selecting the Bootstrap Diode D_{bs}:

The bootstrap diode needs to be able to block the full power rail voltage, which is seen when the MOSFET is switched ON. It must be a fast recovery device to minimize the amount of charge fed back from the bootstrap capacitor into the V_{cc} supply, and similarly the high temperature reverse leakage current would be important if the capacitor has to store charge for long periods of time. The current rating of the diode is the product of the charge calculated

from equation (2.30) and the switching frequency[24].Therefore the diode characteristics :

V_{RPM} : Power voltage rail

$$I_F = Q_{bs} f_s \tag{2.32}$$

2.6.5 Bypass Capacitor C_{Vcc}:

To recharge the bootstrap capacitor;the required charge must be supplied from some larger bypass capacitor, usually the V_{cc}bypass capacitor.This bypass capacitor should be sized to be at least 10 times larger than the bootstrap capacitor so that it is not completely drained during the charging time of the bootstrap capacitor. This allows the bootstrap capacitor to be properly recharged during the charging sequence. This 10x ratio results in 10% maximum ripple on the V_{cc} capacitor in worst case conditions [25].

$$C_{Vcc} \geq 10 C_{bs} \tag{2.33}$$

2.6.6 Gate Resistor R_G:

$R_g$is the gate resistor, which is chosen to optimize switching speed and losses.To calculate the value of the resistor ;the following variables need to be found[26]:

1. The average gate current should be defined:

$$I_{gate(avg)} = \frac{Q_{gs} + Q_{gd}}{t_{sw}} \tag{2.34}$$

- Q_{gs}:Gate-to-Source Charge
- Q_{gd}:Gate-to-Drain (”Miller”) Charge
- t_{sw}:Driver switching time

2. The the total resistance can be expressed as :

$$R_{total} = \frac{V_{CC} - V_{gs(th)}}{I_{gate(avg)}} \tag{2.35}$$

   - $V_{gs(th)}$:Gate Threshold Voltage

3. The driver-ON resistance can be approximated:

$$R_{driver(ON)} = \frac{V_{cc}}{I_{OH+}} \tag{2.36}$$

   - I_{OH+}:the driver Output high short circuit pulsed current

The gate resistance is the difference between the total resistance and the driver ON resistance.

Table 2.1 present the values of the components used in bootstrap circuit

	R_G	C_{Vcc}	C_{bs}
Value	$26.83\,\Omega$	4.2368μ F	$423.68pF$

Table 2.1: Bootstrap's pararmeters

2.7 Maximum Power Point Tracking Algorithms:

MPPT algorithms are necessary in PV applications because the MPP of a solar panel varies with the weather conditions, such as solar irradiation, shadow, and temperature. To extract the maximum power, it is necessary to implement an MPPT algorithm that dynamically adjusts the extraction of the power.

Convergence speed is one of the most important features among all different MPPT algorithms. Such that, any improvement in the rise time of MPPT improves the reliability of the system and increases the power extraction and efficiency of the whole system.

Performance in steady state is also crucial in a PV system; therefore, having fewer oscillations around the MPP will make our system more stable [27].

2.7.0.1 MPPT Techniques Limitations:

Low convergence time and low oscillations in the power response are always desirable from the prospective of good MPPT algorithm. In MPPT algorithms that are going to be expalained , convergence time and the oscillations in power response are directly dependent on perturbation step size. Which makes the selection of step size crucial.
Larger step size in perturbations leads to a smaller convergence time but poor performance in the steady state(large oscillations);and for small step size , the tracking is slow but the oscillations around the MPP are weak[29].

2.7.1 Perturb and Observe "P&O" :

To track and maintain the Maximum Power Point (MPP);P&O algorithm is widely used in the field of photovoltaic (PV) systems due to it simple structure and reduced number of necessary measured parameters.As the name implies, the concept of this method is based on observation of PV panel output power and its perturbation by changing the current or the voltage of PV panel . The algorithm increments or decrements continuously the reference voltage or current based on the previous value of power until it reaches the MPP . When $\frac{dP}{dV}>0$and the operating voltage of PV panel is perturbed in a specific direction, if the perturbation moves the operating point of PV panel to the MPP. P&O method will then continue to perturb the PV voltage in the same direction. When $\frac{dP}{dV}<0$, the perturbation moves the operating point of PV array away from the MPP and the P&O method reverses the direction of the perturbation [28]. Figure 2.12 demonstrate the working principal of this method.
One of the major disadvantage of this technique is in the case of rapid change in atmospheric conditions;this method can move the operating point in the wrong direction and the power losses may be even greater. This incorrect adjustment will continue until the change in irradiance slows down or stabilizes, and before further disturbances are made it is necessary for static converter to operate in steady state.

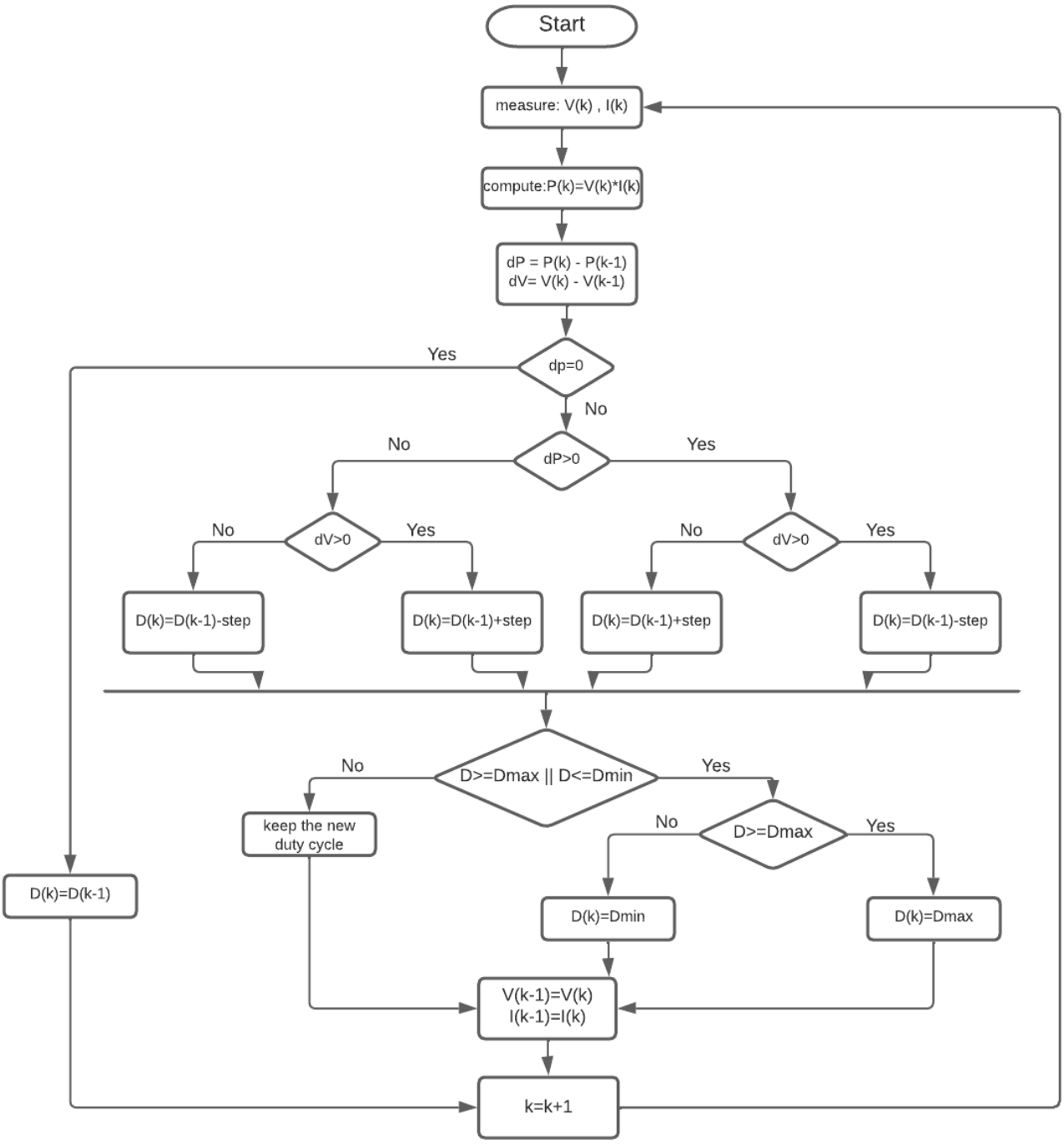

Figure 2.12: perturb and observe flowchart

2.7.2 Incremental Conductance:

The incremental conductance method is one of the widely used conventional MPPT methods [28]. It is based on the slope of the power-voltage relation. The maximum power

occurs at zero slope, whereas negative slope requires voltage decrement and positive slope requires voltage increment to maintain the PV array voltage and power at their optimum values. The following equations summarize the incremental conductance method:

$$P_{PV} = V_{PV} * I_{PV}$$

$$\frac{dP_{PV}}{dV_{PV}} = \frac{d(V_{PV} * I_{PV})}{dV_{PV}} = I_{PV} + V_{PV}\frac{dI_{PV}}{dV_{PV}}$$

At maximum power point $\frac{dP_{PV}}{dV_{PV}} = 0$, this leads to:

$$\frac{I_{PV}}{V_{PV}} = -\frac{dI_{PV}}{dV_{PV}} \tag{2.37}$$

The positioning of the operating point according to the sign of $\frac{dP_{PV}}{dV_{PV}}$ on power characteristic is presented in figure 2.13

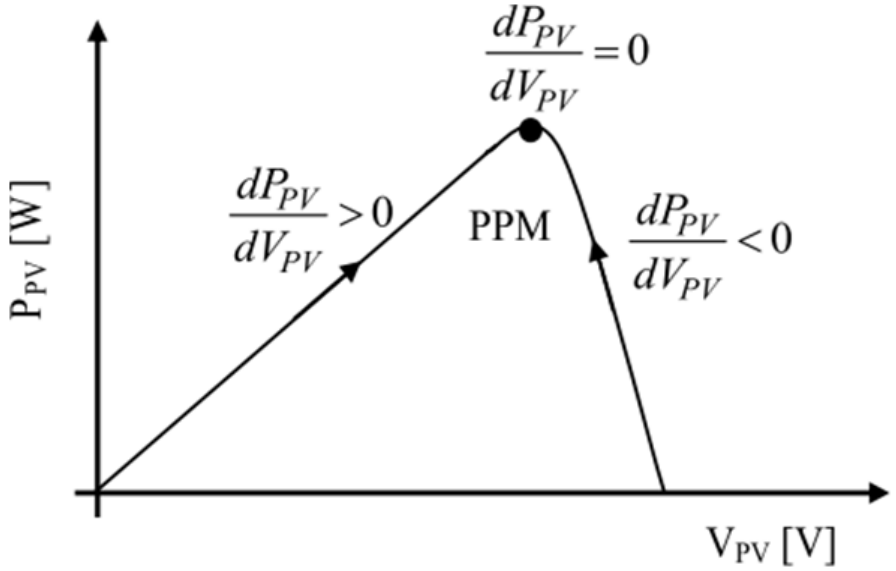

Figure 2.13: Positioning of the operating point according to the sign of $\frac{dP_{PV}}{dV_{PV}}$ on power characteristic

A flowchart of the incremental conductance method for MPPT is in figure 2.14

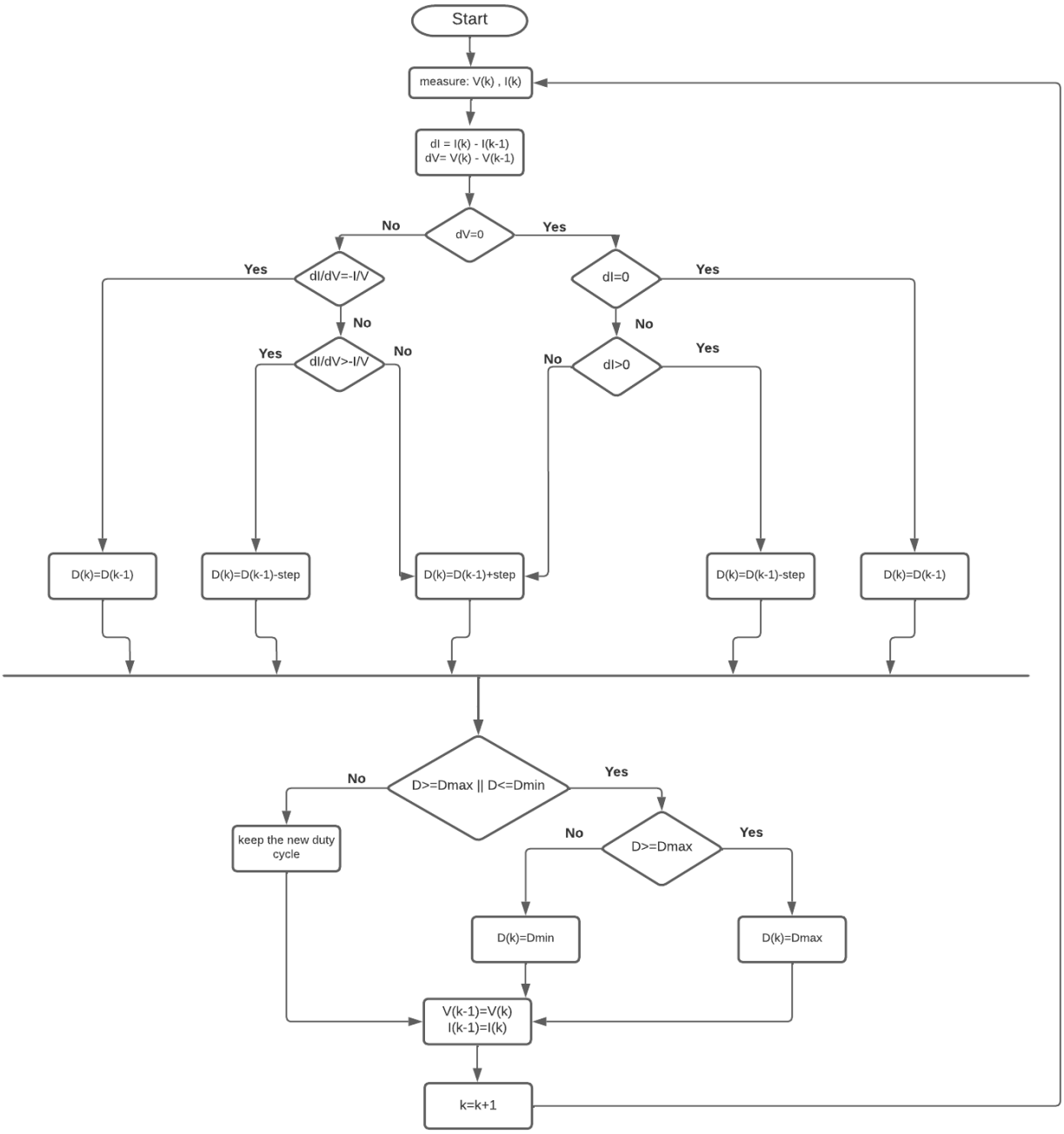

Figure 2.14: incremental inductance flowchart

2.7.3 Fractional Open Circuit Voltage:

The variation in the solar-radiation and the temperature levels given that there is a non linear relationship between $V_{mpp}$and$V_{oc}$of the PV panel has introduce a method known

as FOCV.

$$V_{mpp} = K_{oc} V_{oc} \tag{2.38}$$

$K_{oc}$is a proportionality constant that is dependent on the PV panel characteristics .To determine this constant the values of $V_{mpp}$and V_{oc} need to be known at different environmental conditions. The factorK_{oc} ranges between 0.71 and 0.78 .Once it is known , V_{mpp} will be computed with V_{oc}measured at each iteration by periodically turning OFF the DC-DC converter .However ,this present some disadvantages , including temporary loss of power[30].The working principal of the method is presented in the figure2.15

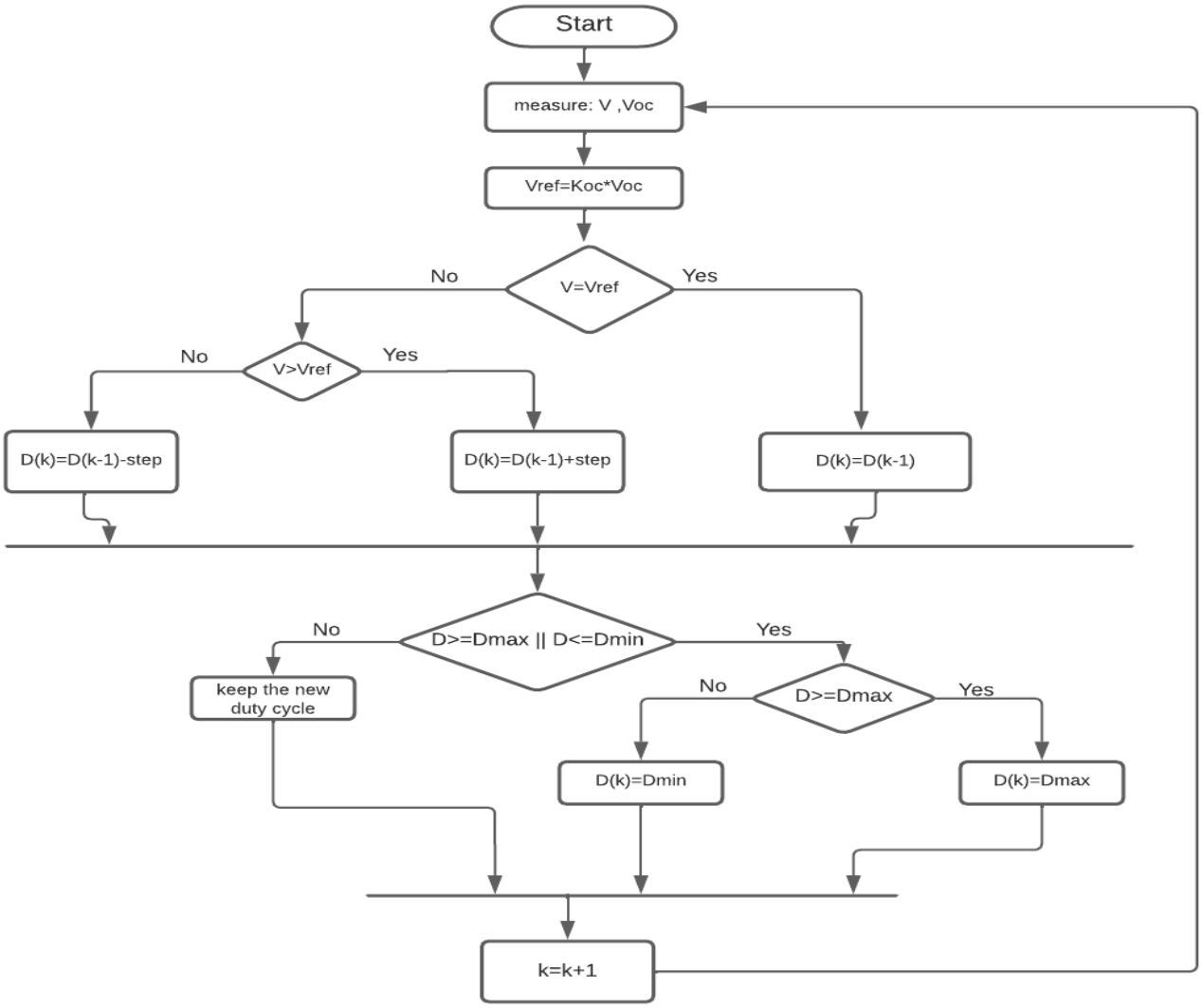

Figure 2.15: FOCV flowchart

2.7.4 Fractional Short Circuit Current:

When the solar-radiation and temperature are not stable and change with time the method fractionalI_{sc} results ,and $I_{mpp}$is approximately linearly related to the $I_{sc}$of the PV panel.

$$I_{mpp} = K_{sc} I_{sc} \tag{2.39}$$

$K_{sc}$is the proportionality constant,this factor is determined according to the PV panel used.K_{sc}vary between 0.78 and 0.92 .Measuring I_{sc} causes an issue therefore and additional switch need to be added to periodically short the PV panel so that the I_{sc} can be measured using a current sensor[30].The working principal of the method is shown in figure 2.16.

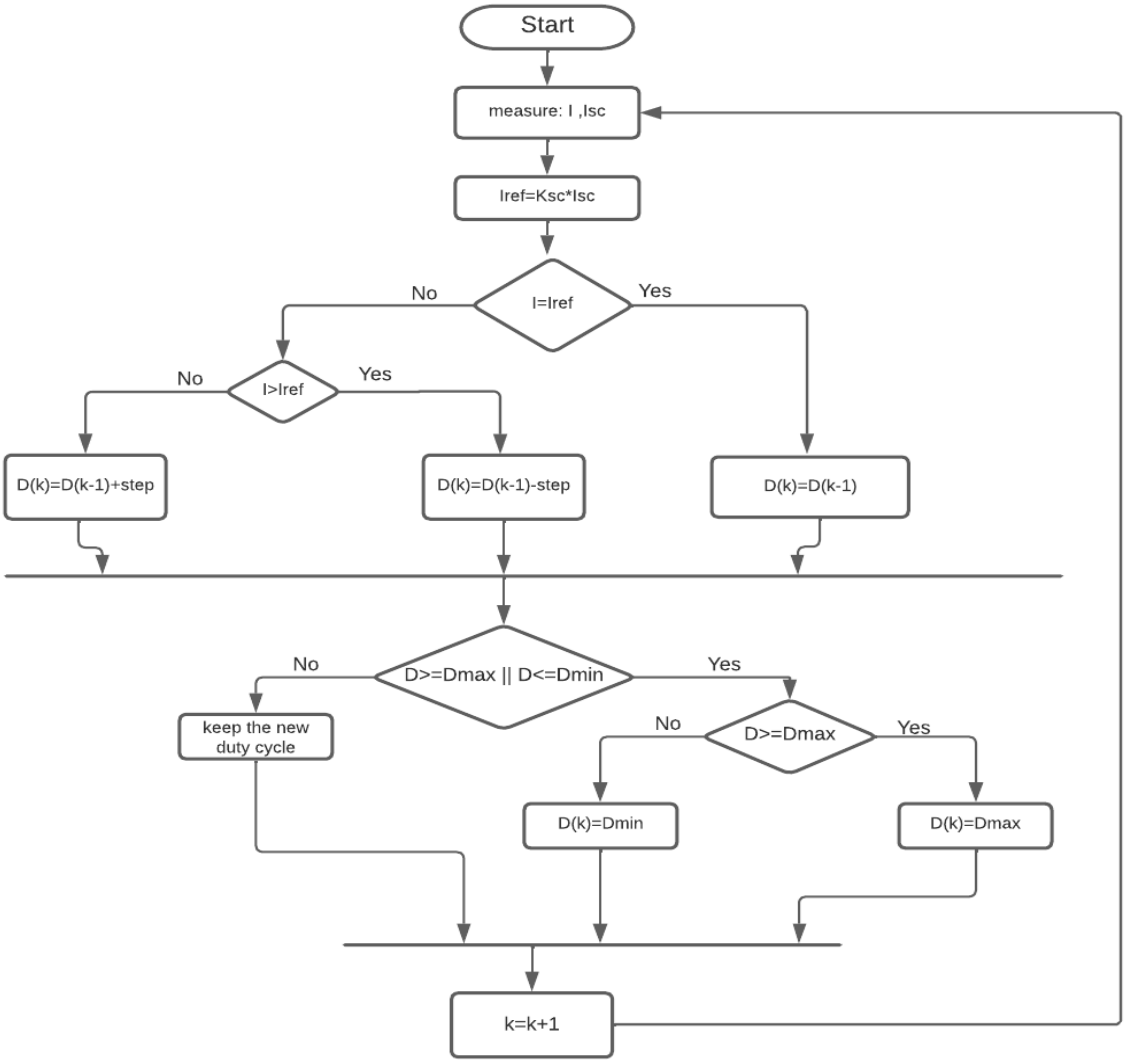

Figure 2.16: FSCC flowchart

2.8 Conclusion:

This chapter has presented the designing method of the buck converter to meet the requirement of the system ;the battery to be used for storing energy and also the bootstrap circuit was explained.Finally ; different MPPT algorithms used to locate the Maximum Power Point of the PV panel have been described;the results of using those techniques will be shown in the upcoming parts .

Chapter 3

Simulation, Results and Discussion

3.1 Introduction:

This chapter focuses on the simulation of a mathematical PV module using Simulink and electrical model using Proteus software. The chapter explores the integration of a Maximum Power Point Tracking (MPPT) techniques and a buck converter for battery charging. By simulating the PV system under various conditions, the efficiency and effectiveness of the system can be evaluated.

3.2 PV Model

3.2.1 Mathematical Model:

A mathematical model of Suntech STP135-12/Tb PV module was developed in Simulink to capture the electrical characteristics and behavior of the PV system under variable conditions. this model is constructed based on the equations mentioned in chapter1 (1.4, 1.5, 1.6, 1.7). The photovoltaic model described can be improved if equation (1.6) is replaced by:

$$I_0 = \frac{I_{\text{sc,n}} + K_i \Delta T}{\exp\left(\frac{V_{\text{oc,n}} + K_v \Delta T}{a V_t}\right) - 1} \tag{3.1}$$

This modification aims to match the open-circuit voltages of the model with the experimental data for a very large range of temperatures as in [5]. this equation is obtained from eq 1.6 by including the current and voltage coefficients K_v and K_i.

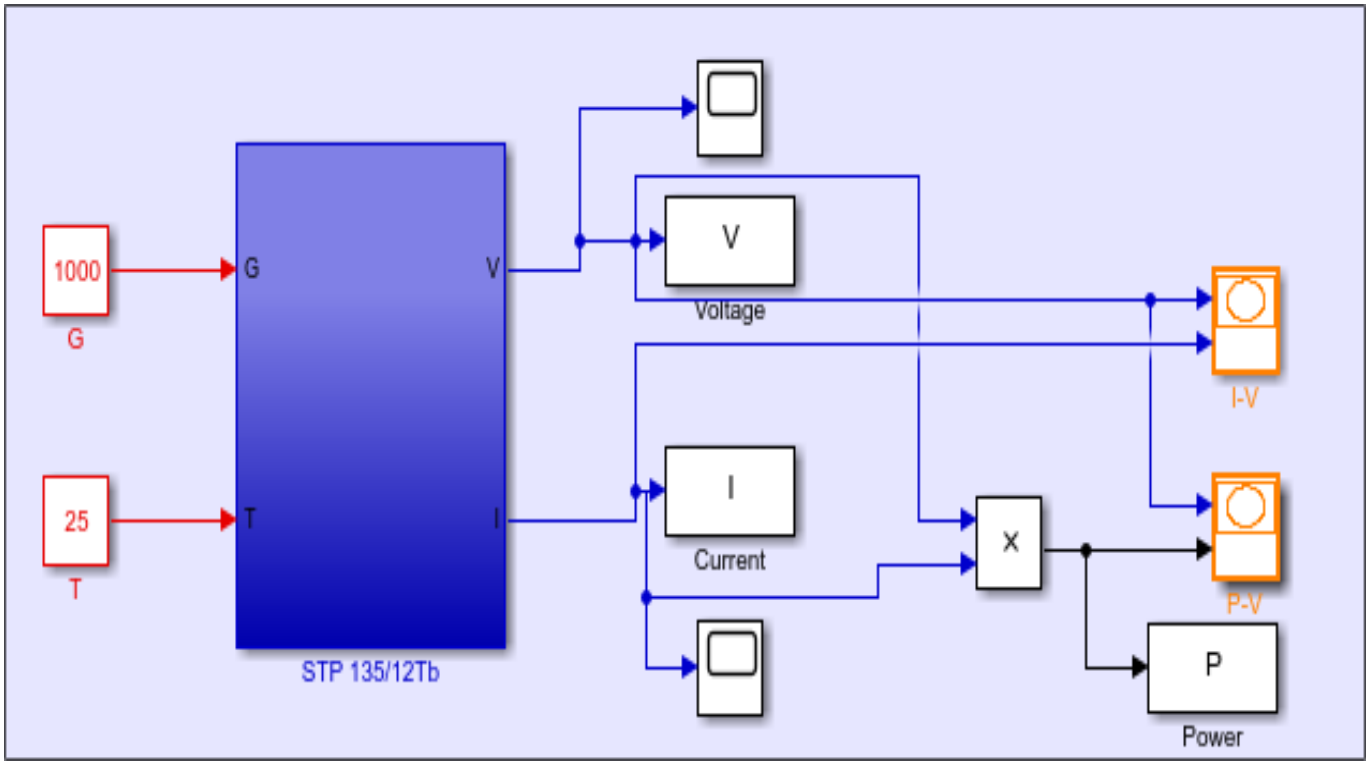

Figure 3.1: Simulink Model of single PV Module

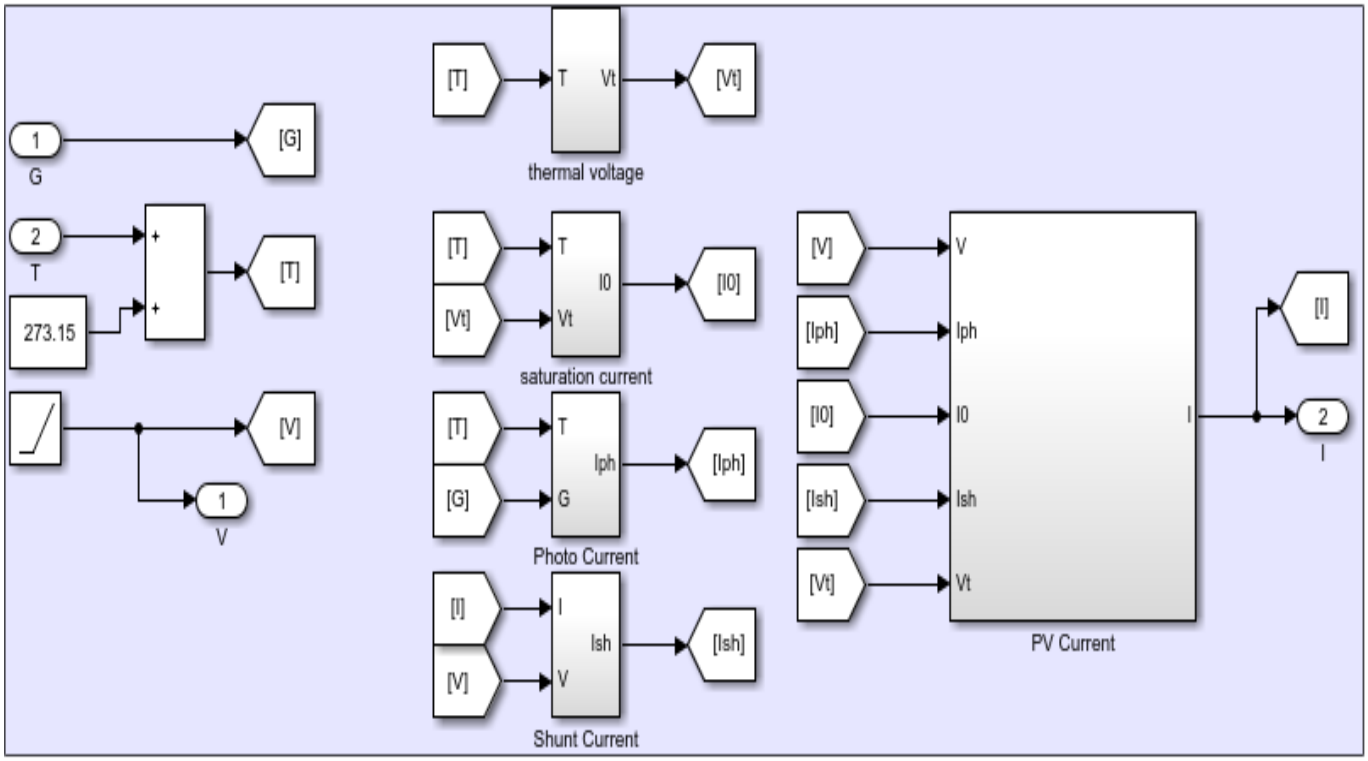

Figure 3.2: Mathematical Model of a single PV Module

3.2.2 Electrical Model:

A model was developed using Proteus software, consisting of a voltage-controlled current source to generate the photocurrent, a diode, and series and parallel resistances. A SPICE script was created to modify the diode's saturation current to our desired value, as seen in Figure 3.3. The values of the elements are specified in Table 3.1.

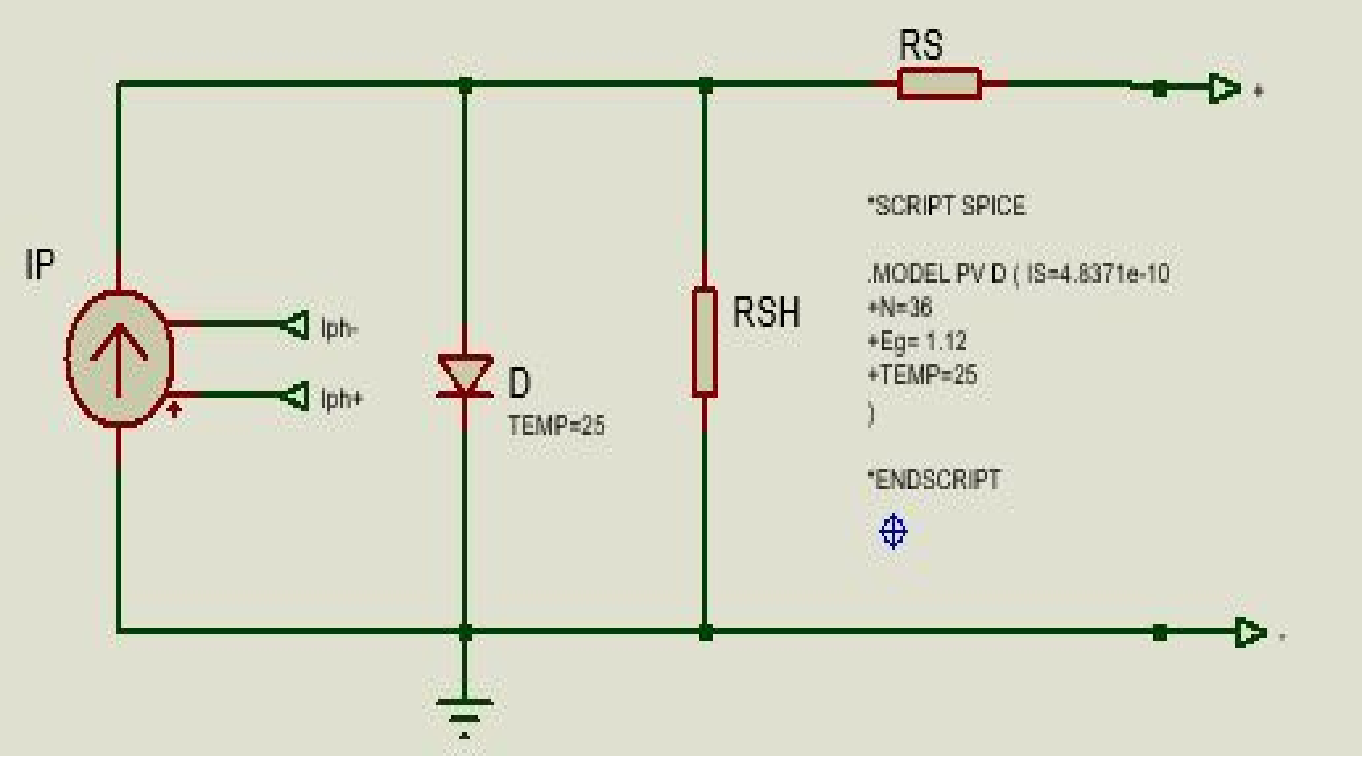

Figure 3.3: Proteus Model of single PV Module

3.3 PV Module Characteristcs:

In this section, Suntech STP135-12/Tb PV module was used. Specifications of the chosen module are presented in table 3.1

Parameter	Symbol	Value
Open-Circuit Voltage	V_{oc}	22.3 V
Short-Circuit Current	I_{sc}	8.2 A
Maximum Power Point Voltage	V_{mpp}	17.5 V
Maximum Power Point Current	I_{mpp}	7.71 A
Maximum Power at STC	P_{max}	$135W_p$
Number of Cells	N_s	36
Short-circuit current temperature coefficient	K_i	0.00055A/K
Temperature Coefficient of Voltage	K_v	-0.075V/K
Diode Ideality Factor	a	1.0235
Saturation Current	I_0	4.8371×10^{-10} A
Shunt Resistance	R_{sh}	414.978572 Ω
Series Resistance	R_s	0.263 Ω
Efficiency	η	13.49%
Fill Factor	FF	0.73827
Dimensions	Length Width Thickness	1.482 m 0.676 m 0.035 m

Table 3.1: PV module specification under STC conditions

3.3.1 Under Normal Conditions:

Figure 3.1 and 3.2 represent a Simulink model of the proposed PV module and figure 3.4 shows its corresponding I-V and P-V curve under STC (G=1000W/m²,T=25°C).

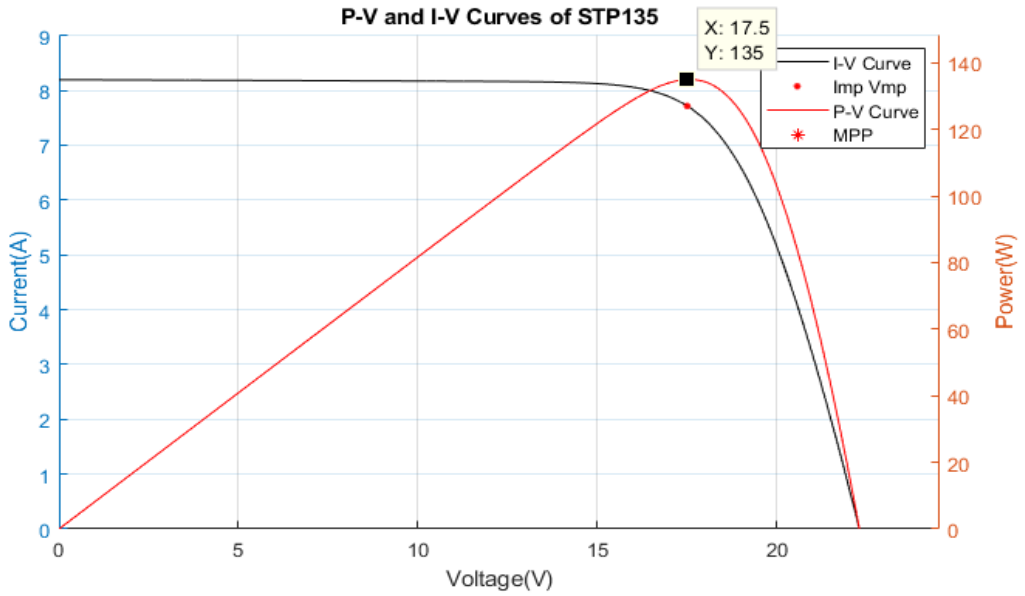

Figure 3.4: I-V and P-V curves under STC

3.3.2 Under Variant Irradiance:

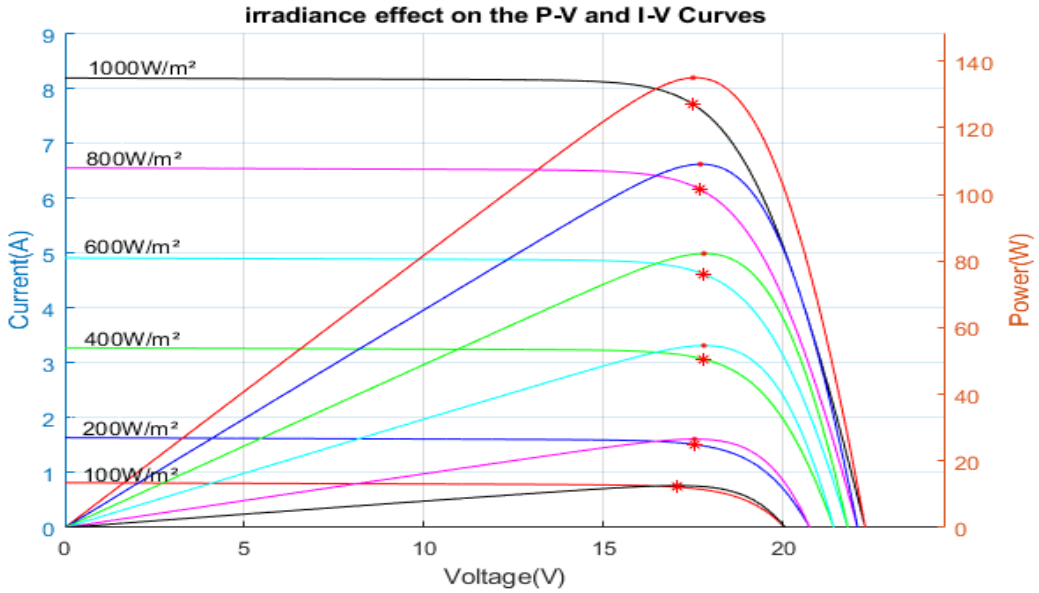

Figure 3.5: Irradiance effect on the I-V and P-V curves

As it can be observed from figure 3.5, there is a direct relationship between irradiance level and the corresponding current output. When irradiance level rises, the current generated by the PV system increases, and vice versa.

3.3.3 Under Variant Temperature:

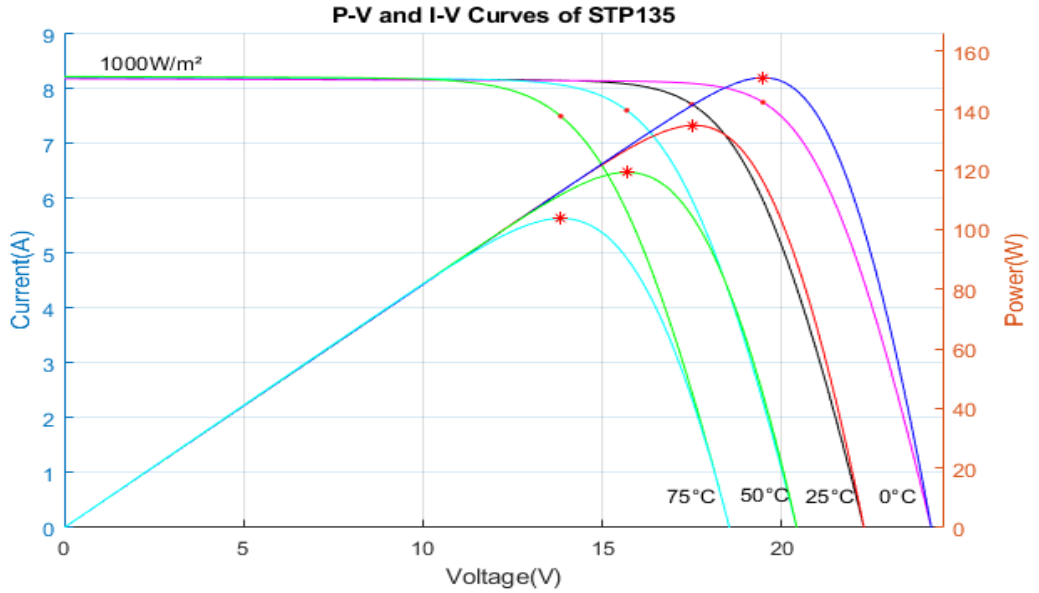

Figure 3.6: Temperature effect on the I-V and P-V curves

As it can be observed from figure 3.6, there is an inverse relationship between temperature level and the corresponding voltage output. When temperature level rises, the voltage output of the PV system decreases, and vise versa.

The following tables illustrate the effects of temperature and irradiance variations on the performance of the photovoltaic module. These tables provide valuable insights into how changing environmental conditions impact specific parameters such as current, voltage, power output, and efficiency. By examining these tables, we can gain a better understanding of the behavior and performance characteristics of the photovoltaic module under different operating conditions.

Irradiance (W/m²)	P_{mpp}	V_{mpp}**(V)**	I_{mpp}**(A)**	V_{oc}**(V)**	I_{sc}**(A)**	**Efficiency** (η)
100	14.186	19.16	0.7404	22.1778	0.8181	14.16 %
200	29.841	19.6	1.5225	22.779	1.636	14.89 %
400	61.184	19.82	3.087	23.3802	3.272	15.268 %
600	91.975	19.8	4.6452	23.7319	4.909	15.3 %
800	121.953	19.66	6.2031	23.9814	6.545	15.216 %
1000	151	19.48	7.7515	24.175	8.181	15.07 %

Table 3.2: PV Panel Performance at T= 0°C with Varying Irradiation

Irradiance (W/m²)	$P_{mpp}(W)$	V_{mp}**(V)**	I_{mp}**(A)**	V_{oc}**(V)**	I_{sc}**(A)**	**Efficiency** (η)
100	12.6	17.06	0.7387	20.12	0.82	12.58 %
200	26.5731	17.54	1.515	20.7762	1.64	13.26 %
400	54.628	17.8	3.069	21.4325	3.28	13.632 %
600	82.22	17.8	4.619	21.8164	4.92	13.678 %
800	109.05	17.7	6.161	22.0887	6.56	13.606 %
1000	135	17.5	7.714	22.3	8.2	13.475 %

Table 3.3: PV Panel Performance at T= 25°C with Varying Irradiation

Irradiance (W/m²)	$P_{mpp}(W)$	V_{mp}**(V)**	I_{mp}**(A)**	V_{oc}**(V)**	I_{sc}**(A)**	**Efficiency** (η)
100	11.02	14.96	0.7366	18.0622	0.821	11 %
200	23.327	15.5	1.505	18.7735	1.6427	11.64 %
400	48.155	15.84	3.0401	19.4847	3.2855	12.05 %
600	72.5875	15.88	4.571	19.901	4.9282	12.0758 %
800	96.33	15.82	6.0891	20.196	6.571	12.02 %
1000	119.246	15.68	7.605	20.425	8.2137	11.903 %

Table 3.4: PV Panel Performance at T= 50°C with Varying Irradiation

Irradiance (W/m²)	$P_{mpp}(W)$	V_{mp}**(V)**	I_{mp}**(A)**	V_{oc}**(V)**	I_{sc}**(A)**	**Efficiency** (η)
100	9.44	12.92	0.731	16.0044	0.8227	9.427 %
200	20.12	13.5	1.4903	16.7707	1.6455	10.04 %
400	41.77	13.9	3.005	17.537	3.291	10.42 %
600	63.107	13.98	4.5141	17.9853	4.9365	10.5 %
800	83.82	13.94	6.013	18.3033	6.582	10.46 %
1000	103.77	13.84	7.4981	18.55	8.2275	10.36 %

Table 3.5: PV Panel Performance at T= 75°C with Varying Irradiation

3.4 Maximum Power Point Tracking System:

In order to extract the maximum power from a PV module to charge a battery, the Simulink model shown in figure 3.7 was simulated.

In this simulation, Perturb and Observe, Incremental Conductance, Fractional Open Circuit, and Fractional Short Circuit techniques were tested. These techniques are responsible for varying the duty cycle, which is used to control the buck converter switch. The values of the buck converter's components were calculated using the sizing equations mentioned in Chapter Two, and it is listed in table 3.6:

Frequency	**Inductor**	**Input Capacitor**	**Output Capacitor**
31.37255kHz	57.97 μ H	481.76 μ F	97.49μ F

Table 3.6: Buck Converter's pararmeters

The simulation offers an opportunity to verify the performance of the proposed algorithms. For evaluation and comparative analysis, the simulation studies were carried out under steady-state and dynamic conditions.

The PV panel was expected to produce 135W with MPPT voltage and current of 17.5V and 7.71A respectively at 1000 W/m² solar irradiance and 25°C. In order to study the performance of the algorithms under climate changing conditions the irradiance and temperature signals were varied as shown in figure 3.8.

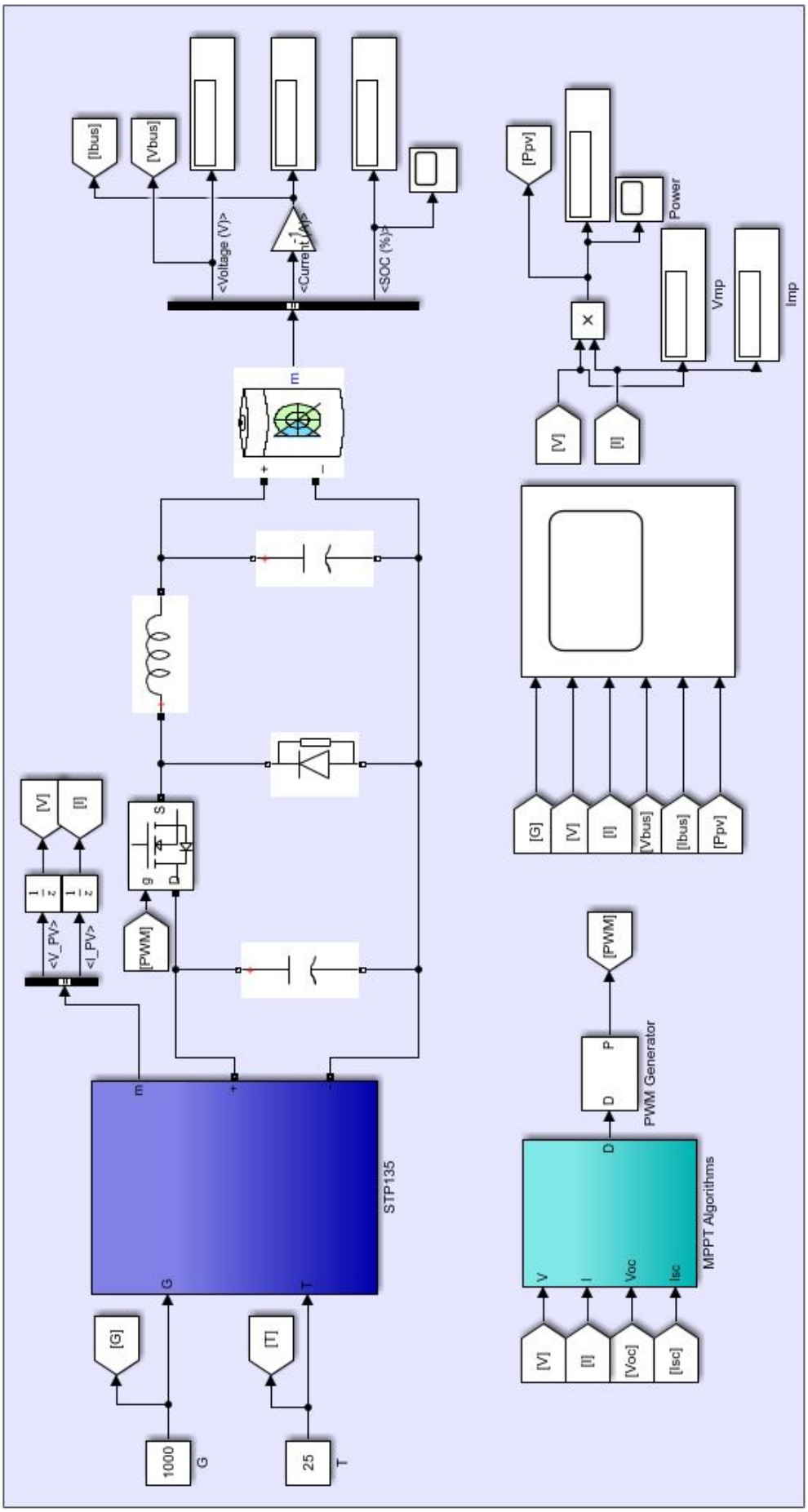

Figure 3.7: PV system for charging a battery

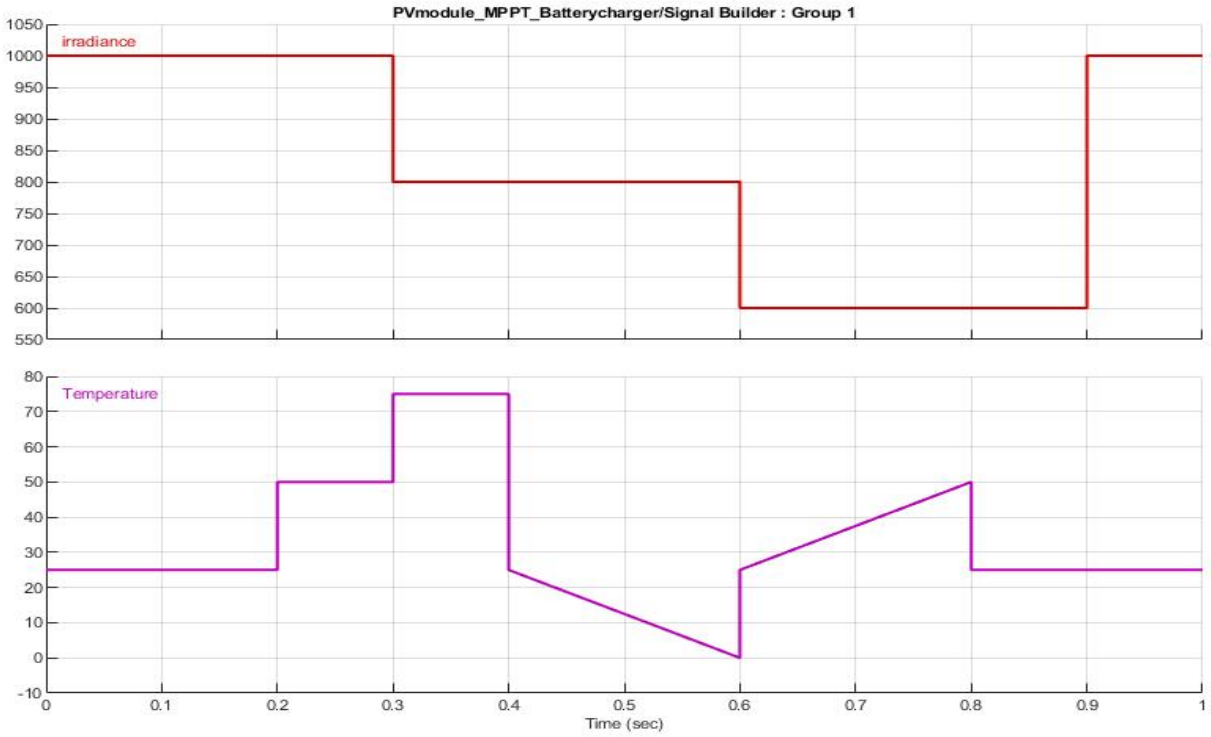

Figure 3.8: Irradiance and Temperature signals

3.4.1 Perturb and Observe Algorithm Simulation:

The conventional Perturb and Observe algorithm, introduced in Chapter Two, was implemented as an M-file code based on its algorithm in an embedded MATLAB function.
The initial values of the P&O parameters were defined in table 3.7.

Dinit	**Dmax**	**Dmin**	**deltaD**
0.6	0.9692	0.555	0.01 and 0.001

Table 3.7: Perturbe and Observe

The simulation results of the PV system presented in figure 3.7 with P&O algorithm under uniform conditions are shown in figures from 3.9 and 3.10.

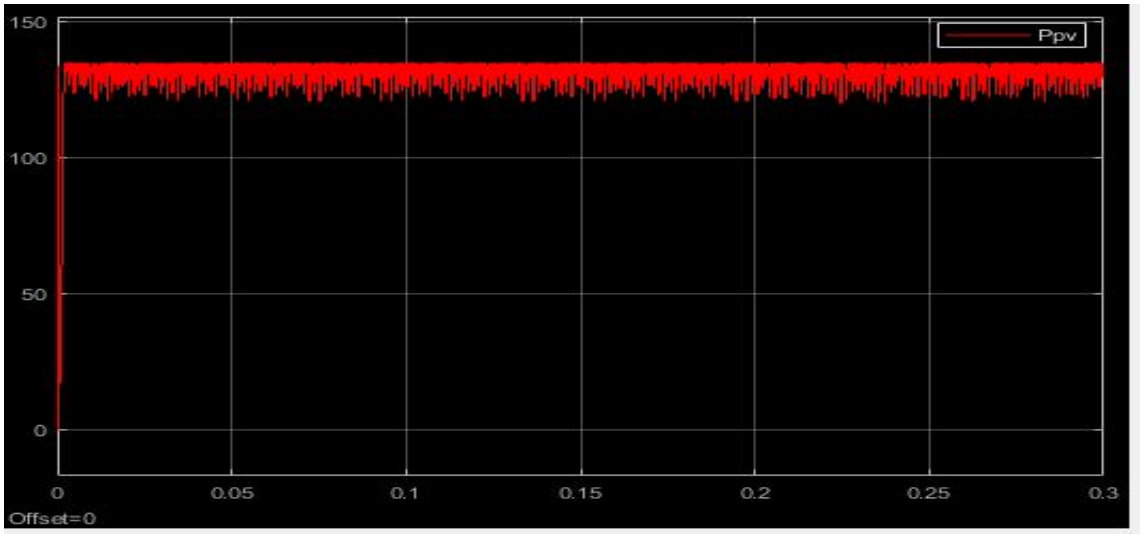

Figure 3.9: Power waveform using P&O under STC with large step size

By changing the step size to a lower value we get the following results:

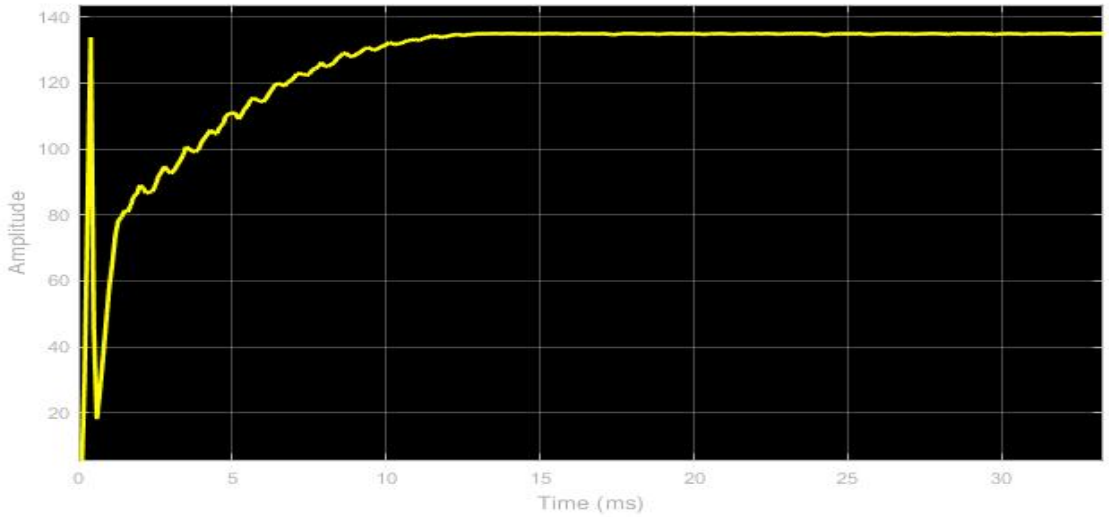

Figure 3.10: Power waveform using P&O under STC with small step size

The simulation results demonstrate the P&O algorithm's effectiveness in tracking the maximum power point (MPP). The algorithm exhibits a small convergence time to reach the steady state when using a large step size, taking approximately 2.1ms to reach the MPP. However, this configuration is associated with higher oscillations around the MPP. On the other hand, when employing a small step size, the algorithm yields to smoother response around the MPP but requires longer convergence time of 13ms.

The simulation of the model under varying irradiation and Temperature levels (figure 3.8) gives

the resulting waveform shown in figures 3.11.

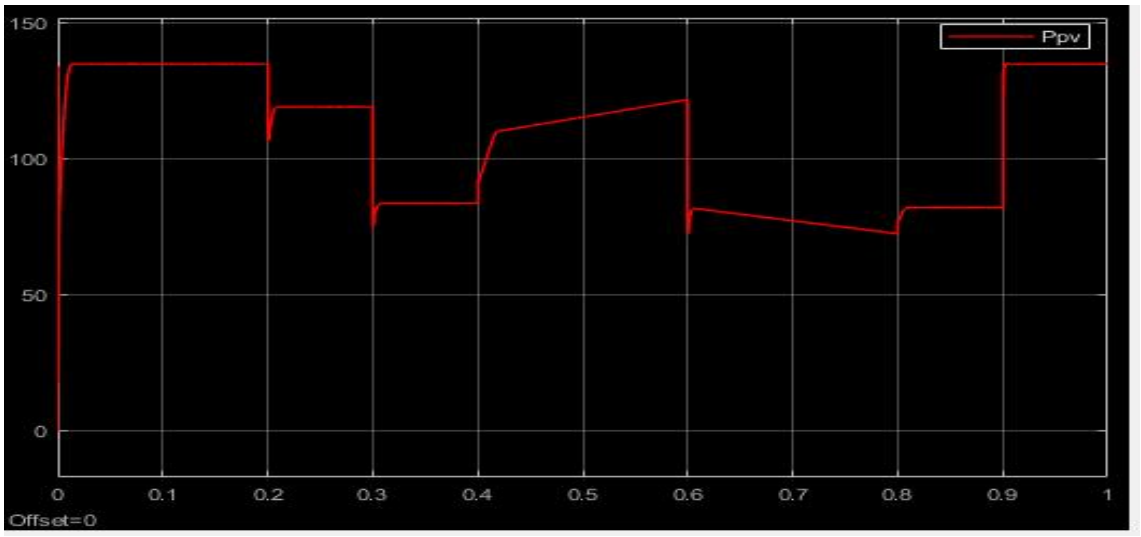

Figure 3.11: Power waveform using P&O under variant environmental conditions with small step size

As seen from Figure 3.11, the P&O algorithm can track the MPP during changes in irradiance or temperature levels. It can be observed that the algorithm loses track and then immediately restarts to find the new MPP due to the sudden change in environmental conditions.

3.4.2 Incremental Conductance Algorithm Simulation:

the conventional Incremental Conductance algorithm, introduced in Chapter two, was implemented as an M-file code based on its algorithm in an embedded MATLAB function. The initial values The initial values of the IC parameters were defined in table 3.7.
The simulation result of the PV system presented in figure 3.7 with MPPT IC algorithm under uniform conditions are shown in figure 3.12.

The simulation results demonstrate the IC algorithm's effectiveness in tracking the maximum power point (MPP).

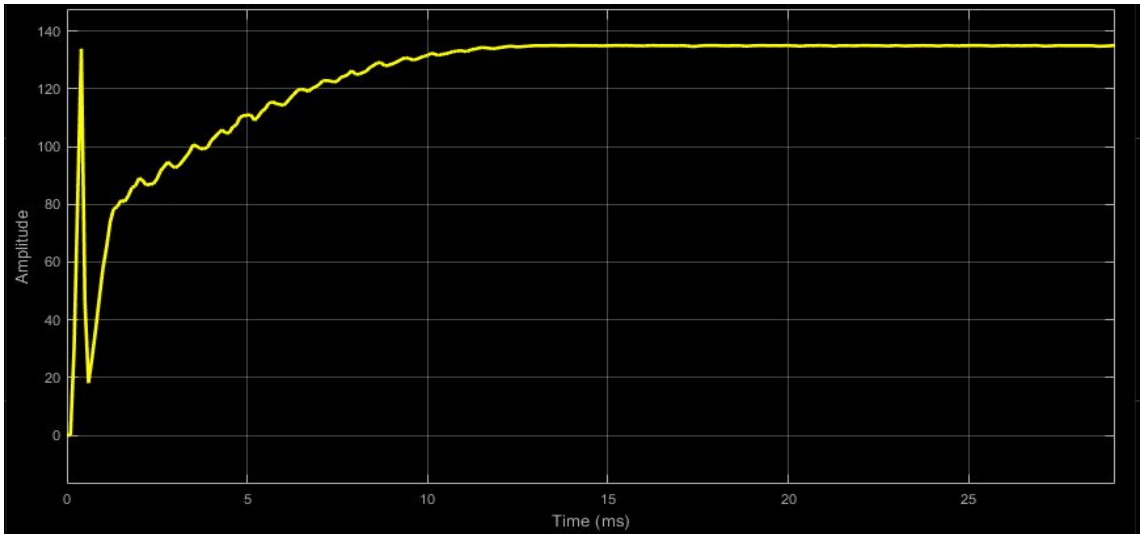

Figure 3.12: Power waveform using IC under STC

The simulation of the model under varying irradiation and Temperature levels (figure 3.8) gives the resulting waveform shown in figures 3.13.

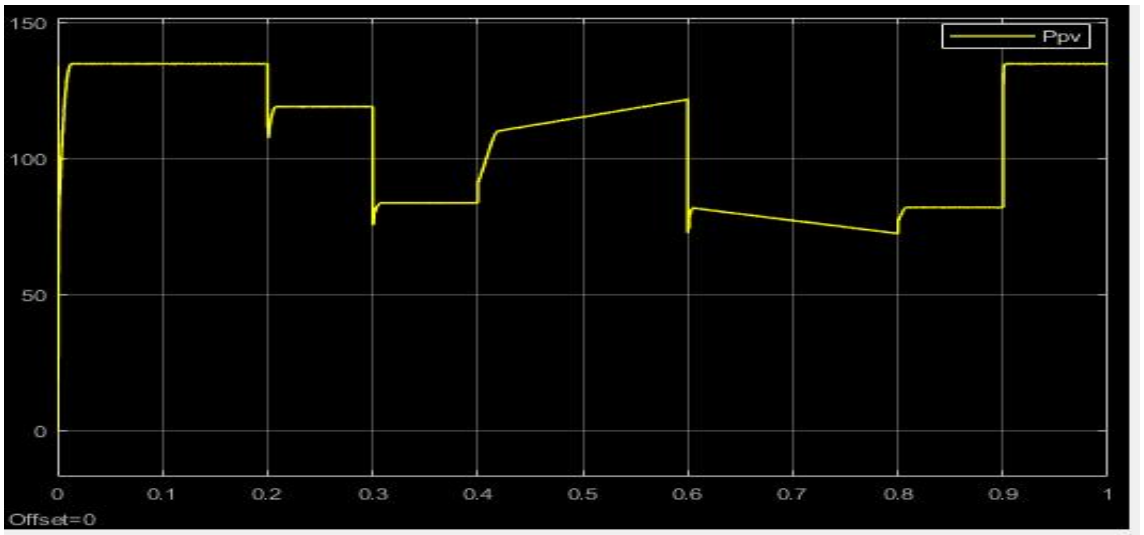

Figure 3.13: Power waveform using IC under variant environmental conditions

As seen from figure 3.11, the IC algorithm can track the MPP during changes in irradiance or temperature levels. It can be observed that the algorithm loses track and then immediately restarts to find the new MPP due to the sudden change in environmental conditions.

3.4.3 Fractional Open Circuit Voltage and Short Circuit Current:

The Fractional Open Circuit Voltage (FOCV) and Short Circuit Current (FSCC) algorithms, introduced in Chapter Two, were implemented as an M-file code based on their respective algorithms in an embedded MATLAB function. The initial values of the FOCV and FSCC parameters were defined in Table 3.7, with k_{oc}=0.78 and k_{sc}=0.94.

The simulation results of the PV system with FOCV and FSCC algorithms under uniform conditions show their effectiveness in tracking the MPP as seen in figure 3.14. However, these two algorithms failed to find the MPP under certain conditions when varying the irradiance and temperature levels. This limitation can be attributed to the open circuit and short circuit factors present in the algorithms.

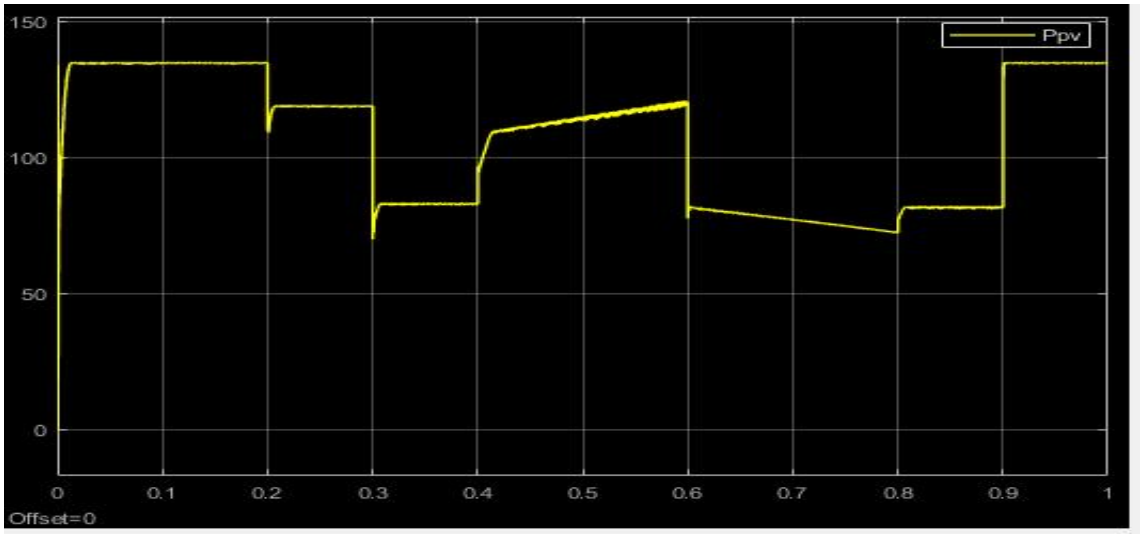

Figure 3.14: Power waveform using CV under variant environmental conditions

3.4.4 Battery Charging Process:

In the simulation, the battery block used was sourced from the Simulink/Simscape library. The characteristics of the used battery are shown in table 4.2. in order to show that the battery is charging when the simulation is running and due to some limitation, the simulation ran for 2 minutes and the following figure shows the battery state of charge.

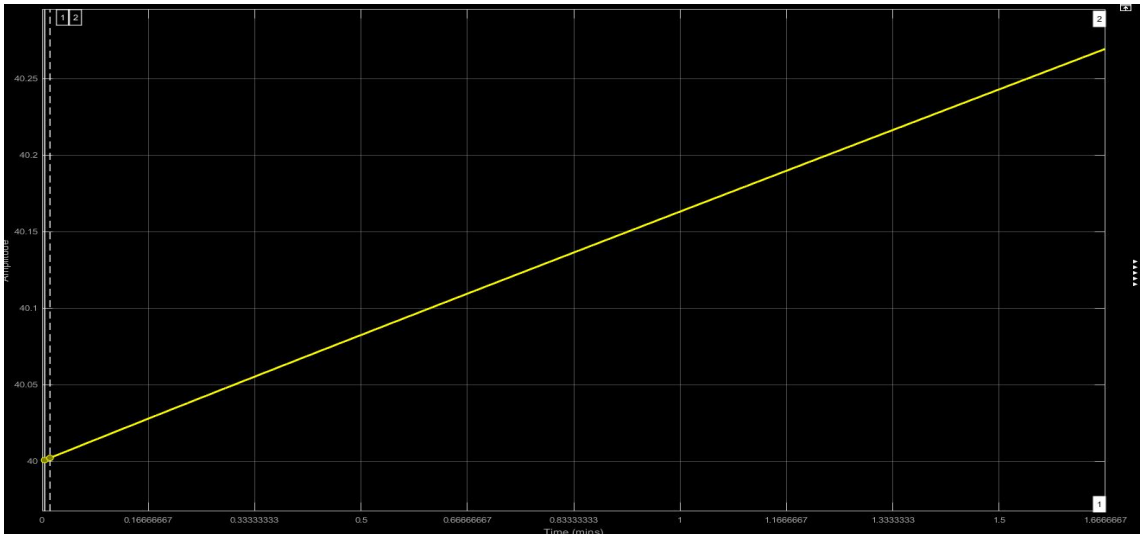

Figure 3.15: State of charge of the battery

3.5 Detailed Comparison and Discussion of the Four Algorithms:

The following table demonstrates the performance of the different used MPPT techniques under standard conditions, the PV module is suppose to produce 135W:

/	P&O	IC	FOCV	FSCC
Extracted Pmpp	134.8045W	134.88W	134.72W	134.77W
Efficiency	99.855%	99.91%	99.79%	99.829%
Tracking time	13ms	13ms	13.4ms	13.4ms

Table 3.8: Comparison of different MPPT Techniques under Standard Conditions

It can be observed from Table 3.8 that both the IC and P&O techniques exhibit faster convergence to the steady state compared to the FOCV and FSCC techniques. However, the Incremental Conductance technique tends to demonstrate better efficiency compared to the other three techniques, as it exhibits less perturbation around the MPP.

To demonstrate the performance under variant environmental conditions and compare the proposed techniques, the following tables provide the necessary data:

Irradiance(W/m²)	Temperature(°C)	Extracted Pmpp(W)	Efficency (%)	Tracking time(ms)
1000	50	119.1435	99.91	8.287
800	75	83.7875	99.95	8.068
600	25	82.11	99.868	8.687
1000	25	134.8045	99.855	3.271

Table 3.9: P&O algorithm performance under variant temperature and irradiation

Irradiance(W/m²)	Temperature(°C)	Extracted Pmpp(W)	Efficency (%)	Tracking time(ms)
1000	50	119.1765	99.94	8.185
800	75	83.791	99.965	7.951
600	25	82.11	99.868	8.217
1000	25	134.825	99.91	2.317

Table 3.10: IC algorithm performance under variant temperature and irradiation

Irradiance(W/m²)	Temperature(°C)	Extracted Pmpp(W)	Efficency (%)	Tracking time(ms)
1000	50	118.907	99.714	10.363
800	75	83.015	99.038	10.345
600	25	81.647	99.305	12.8
1000	25	134.735	99.79	1.5

Table 3.11: FOCV algorithm performance under variant temperature and irradiation

Irradiance(W/m²)	Temperature(°C)	Extracted Pmpp(W)	Efficency (%)	Tracking time(ms)
1000	50	118.93	99.73	8.4
800	75	83.276	99.35	11.213
600	25	82.1	99.856	9.346
1000	25	134.77	99.829	2.592

Table 3.12: FSCC algorithm performance under variant temperature and irradiation

As seen from Tables 3.9 to 3.12, all algorithms demonstrate satisfactory performance and can effectively track the maximum power point under changing environmental conditions. However, the incremental conductance technique exhibits the best tracking speed and power output compared to the other three techniques. The Perturb and Observe (P&O) and Incremental Conductance (IC) techniques show similar tracking times for small changes in operation. However, for significant variations, the IC technique outperforms the P&O technique, showing better tracking capabilities. In contrast, the fractional open circuit voltage (FOCV) and fractional short circuit current(FSCC) techniques have the longest tracking time in general. However, it is interesting to note that in the last irradiance and temperature change scenario, the

FOCV and FSCC techniques exhibited the lowest tracking time, even surpassing the tracking time of the IC and P&O techniques. This indicates that the open circuit and short circuit coefficients were well-suited for that specific combination of irradiation and temperature conditions. It can be concluded that the performance of these techniques is influenced by the environmental factors, and optimal results can be achieved when the coefficients align well with the irradiance and temperature levels.

3.5.1 Discussion:

The IC technique stands out as a favorable choice due to its fast tracking speed and accurate adjustments based on derivative information. It is excellent in scenarios with significant variations in operating conditions, allowing it to quickly adapt to changing environmental factors. This results in efficient power extraction and improved overall system performance and gives it an advantage over the P&O, FOCV, and FSCC techniques.

While the P&O technique is widely used and relatively simple to implement, it can suffer from slow convergence and oscillations around the MPP due to its reliance on perturbing the operating point and observing the resulting change in power. In contrast, the IC technique's use of derivative information enables it to overcome these limitations, providing faster and more precise tracking of the maximum power point.

On the other hand, the FOCV and FSCC techniques use the ratio between the open circuit voltage and the voltage at the MPP, as well as the short circuit current and the current at the MPP, respectively, to estimate the maximum power point. These techniques offer benefits in certain scenarios where the open circuit and short circuit coefficients align well with the irradiance and temperature conditions. However, they generally exhibit longer tracking times and may not perform as effectively in dynamic environments or when facing rapid changes in operating conditions.

Considering the overall performance, IC emerges as a reliable and efficient choice for MPPT in PV systems. Its fast tracking speed, accurate adjustments, and ability to adapt to varying conditions make it well-suited for applications where real-time tracking and optimal power extraction are essential. However, it is important to assess the specific requirements and

characteristics of the PV system and the operating conditions to determine the most suitable MPPT technique.

In summary, while each technique has its strengths and weaknesses, the IC technique offers a combination of fast tracking speed, accurate adjustments, and adaptability that make it a preferred choice for effective MPPT in a wide range of PV system applications.

3.6 Implementation of the MPPT System Using Proteus Software:

Proteus software was chosen for implementing the desired system due to its helpful features. It offers a wide range of components for accurately simulating the system, including microcontrollers. Proteus has an easy-to-use interface for designing circuits and provides real-time analysis, making it easier to evaluate system performance. It also supports the simulation of microcontrollers, allowing for control algorithms integration.Additionally, Proteus provides the flexibility to model custom components, such as the unique PV model used in this project. Overall, Proteus offers an effective platform for simulating and testing the desired system shown in figure 3.16.

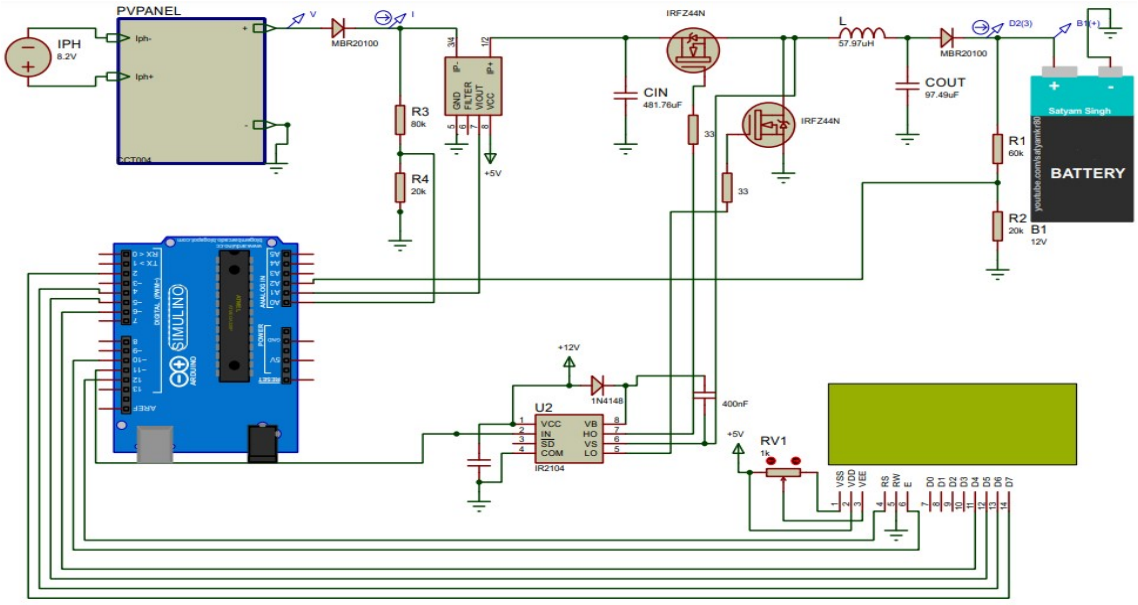

Figure 3.16: MPPT System

The design of this system consists of a PV module, power circuit, control circuit, and sensors for accurate monitoring. The PV module serves as the energy source, while the power circuit includes a DC-DC buck converter to adjust the PV module output for battery storage. Two blocking diodes have been added at the input and output of the converter to prevent the battery from been discharged and protect the power circuit. The control circuit consists of a microcontroller (Arduino UNO in this case). Additionally, sensors were integrated into the system to provide real-time feedback on parameters such as voltage and current, enabling precise monitoring of the PV module performance.

The Perturb and Observe(P&O) algorithm was chosen to be tested in this system. It was implemented using the Arduino IDE, and its purpose is to continuously track and adjust the operating point of the PV module to maximize the power output. The algorithm generates the duty cycle for the PWM signal, which is then driven by the driver to power the converter's switches enabling precise control over the power flow of the system. Finally the values of the voltage, current, and Power will be displayed on the LCD.

3.7 Conclusion:

The simulations offered a valuable opportunity to verify the feasibility and the performance of the proposed PV system. For evaluation and comparison analysis, the simulation studies were carried out under exactly the same conditions for the proposed four algorithms. The results proved that the IC is better than P&O, FOCV and FSCC under normal and changing conditions. Finally a Design of the proposed System was shown and explained. The components used in the implementation of this system is explained in the following chapter.

Chapter 4

Hardware implementation

4.1 Introduction:

This chapter present the component used in the implementation part and the connection between the control circuit and power circuit to ensure the best possible execution of the project .

4.2 Arduino Uno Microcontroller:

The Arduino Uno is an open-source microcontroller board based on the Microchip ATmega328P microcontroller (MCU) and developed by Arduino.cc and initially released in 2010. The board is equipped with sets of digital and analog input/output (I/O) pins that may be interfaced to various expansion boards (shields) and other circuits. The board has 14 digital I/O pins (six capable of PWM output), 6 analog I/O pins, and is programmable with the Arduino IDE (Integrated Development Environment), via a type B USB cable. It can be powered by a USB cable, AC-to-DC adapter or battery to get started[31]. Figure 4.1 demonstrates the Pin diagram .

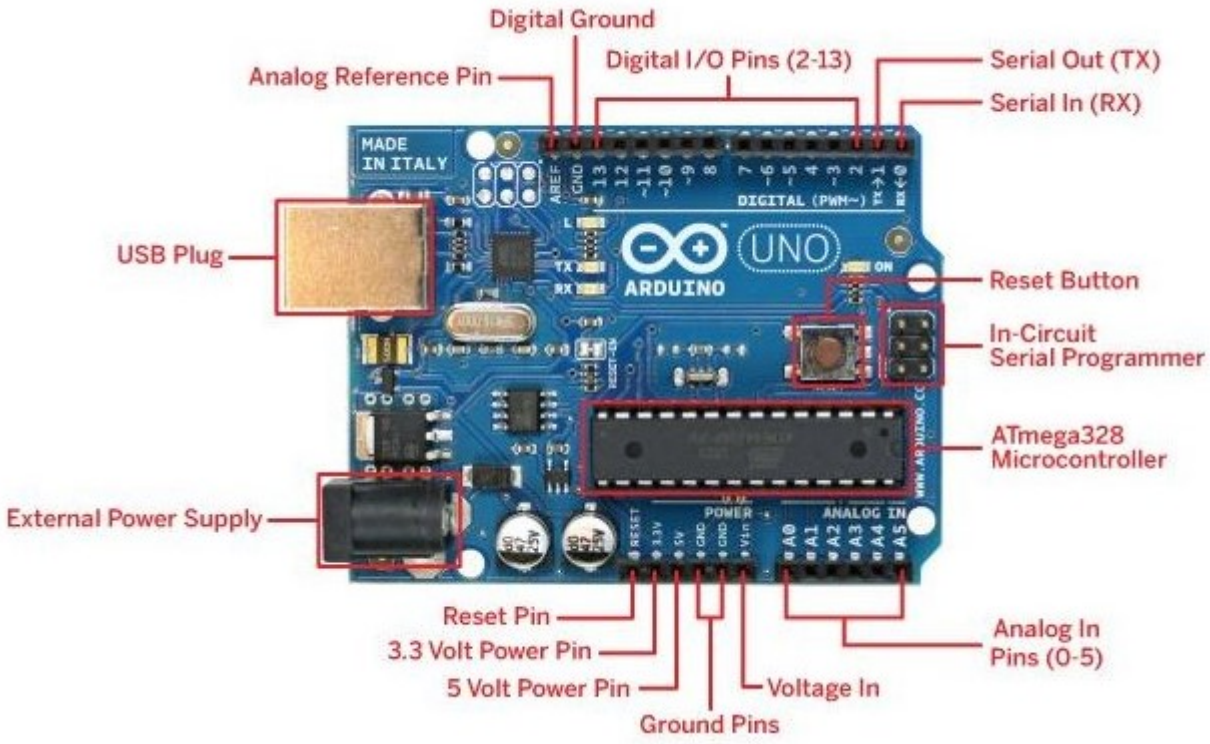

Figure 4.1: Arduino-Uno Pin-Diagram

- **Arduino Uno Base Frequency[32]:** the base frequency of the microcontroller is defined as:

  a) Pins 3 and 11:490.20 Hz

  b) Pins 5 and 6: 976.59 Hz

  c) Pins 9 and 10 :490.20 Hz

  If the desired frequency is another one than the base frequency ,there exist a way to change it by multiplying with some factors to increase the frequency:

  - Allowed factors for pin 3 and 11 are: 1, 8, 32, 64, 128, 256, 1024.
  - Allowed factors for pin 9 and 10 are: 1, 8, 64, 128, 256, 1024.
  - Allowed factors for pin 5 and 6 are: 1, 8, 64, 128, 256, 1024.

4.2.1 Arduino IDE:

The Arduino Integrated Development Environment (IDE) is a cross-platform application (for Windows, macOS, Linux) that is written in functions from C and C++. It is designed for programming and developing applications for Arduino microcontrollers. It provides an interface to write, compile, and upload code to Arduino boards .It includes a code editor with features like syntax highlighting, code completion, and error checking, which aid in writing and debugging Arduino programs.It also provides a library manager,offering a wide range of libraries [31].

4.3 Current Sensor:

ACS712ELCTR-30A-T current sensor consists of a precise, low-offset, linear Hall sensor circuit with a copper conduction path located near the surface of the die. Applied current flowing through this copper conduction path generates a magnetic field which is sensed by the integrated Hall IC and converted into a proportional voltage.The maximum AC or DC that can

be detected can reach 30A, and the present current signal can be read via analog I / O port of Arduino [33].

Specification:

- Supply Voltage: 4.5V 5.5V DC
- Sensitivity: 66mV/A

Figure 4.2 demonstrates the pin-out of the ACS712ELCTR-30A-T

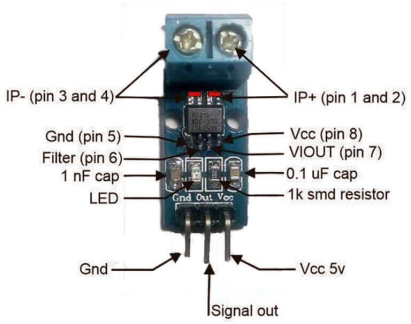

Figure 4.2: ACS712ELCTR-30A-T current sensor

4.4 Voltage Sensor :

The voltage sensor is a simple module that can be used with Arduino (or any other microcontroller with a 5V input tolerance) to measure external voltages higher than its maximum acceptable value, which is 5V in the case of Arduino[34].

Figure 4.3 present the voltage sensor

Figure 4.3: Voltage sensor

4.5 Half-Bridge Driver:

The IR2104(S) are high voltage, high speed power MOSFET and IGBT drivers with dependent high and low side referenced output channels. Proprietary HVIC and latch immune CMOS technologies enable ruggedized monolithic construction. The logic input is compatible with standard CMOS or LSTTL output, down to 3.3V logic. The output drivers feature a high pulse current buffer stage designed for minimum driver cross-conduction. The floating channel can be used to drive an N-channel power MOSFET or IGBT in the high side configuration which operates from 10 to 600 volts[35].

Figure 4.4 show the driver pin-out,and the table 4.1 describes the function of each pin .

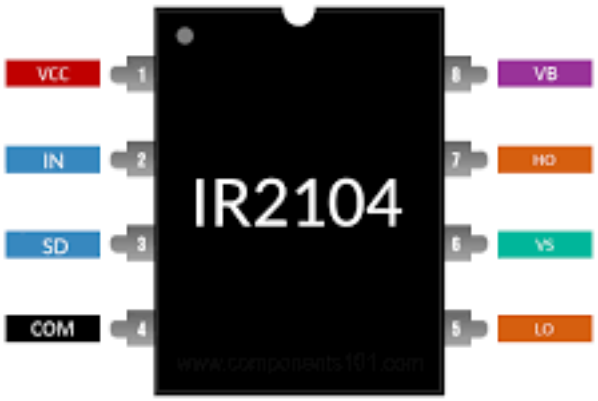

Figure 4.4: IR2104(S) driver pin-out

Symbol	Description
IN	Logic input for high and low side gate driver outputs (HO and LO),in phase with HO
$\overline{SD}$	Logic input for shutdown
V_B	High side floating supply
HO	High side gate drive output
V_S	High side floating supply return
V_{CC}	Low side and logic fixed supply
LO	Low side gate drive output
COM	Low side return

Table 4.1: Pins definition [35].

4.6 Battery:

RA12-100(12V100Ah)series is a general purpose battery with 12 years design life in float service. It meets with international standards. With advanced AGM (Absorbed Glass Mat) valve regulated technology and high purity raw material, the RA series battery maintains high consistency for better performance and reliable standby service life. It is suitable for UPS(Uninterruptible Power Supply)/EPS(Emergency Power Supply), Telecom, power grid, medical equipment, emergency light and security system applications[36]. Figure 4.5 present the battery.

Figure 4.5: RA12-100 battery

Cell Per Unit	6
Voltage Per Unit	12
Nominal Capacity	100Ah@10hour-rate to 1.80V per cell @25°C
Weight	Approx. 27.5 Kg (Tolerance±3.0%)
Internal Resistance	Approx. 6.5 mΩ
Max. Discharge Current	1000A (5 sec)
Short Circuit Current	2150A
Design Life	12 years
Max. Charging Current	30.0 A
Standby Use Voltage	13.6 V 13.8 V @ 25°C Temperature Compensation: -3mV/°C/Cell
Cycle Use Voltage	14.6 V 14.8 V @ 25°C Temperature Compensation: -4mV/°C/Cell

Table 4.2: Battery specification[36]

4.7 Inductance:

An inductor is a passive electronic component that stores energy in the form of a magnetic field when an electric current flows through it. It consists of a coil or winding of wire that may be wound around a core made of a magnetic material.Inductors are characterized by their inductance, which is a measure of their ability to store energy in the magnetic field. Inductance is typically represented by the symbol L and is measured in henries (H)[37].

4.7.1 Self-Made Inductance Calculation of a Ferrite Toroid Coil:

Using the following equation;the number of turns of the coil can be determined[37] :

$$L = \frac{N\phi_B}{I} = \frac{\mu_0 \mu_r N^2}{2\pi} h \log_e(\frac{r_o}{r_i}) \tag{4.1}$$

- N : the number of turns of the coil
- μ_0 :magnetic constant $4\pi 10^-7$[T · m / A]
- μ_r :actual relative magnetic permeability of the core
- I :the value of current through the coil [A]
- r : radius [m]
- r_o :outer radius of the core [m]
- r_i: the inner radius of the core [m]
- h : core height [m]
- L : inductance [H]
- B : magnetic flux density [T]
- ϕ_B: magnetic flux [Wb]

Figure 4.6 shows the self-made inductor

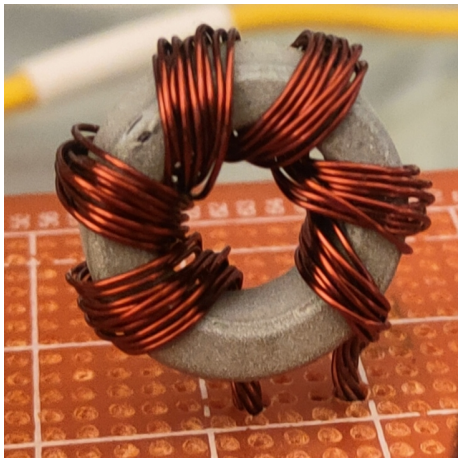

Figure 4.6: self-made inductor

4.8 Supplementary Components :

- **Resistor**:A resistor is an electrical component that limits or regulates the flow of electrical current in an electronic circuit . It is a device that resists the flow of electric current by providing resistance, thereby developing a drop in voltage across the device. The resistance is measured in ohms (Ω)[38].

  The used values:100Ω

- **Diodes:** A diode is a two-terminal semiconductor device that allows current to flow through in one direction only . It is a specialized electronic component that acts as a one-way switch, conducting electric current in only one direction and restricting current from the opposite direction. A diode has two terminals, the anode and the cathode. The anode is indicated in a circuit diagram by the arrowhead, whereas the cathode forms the other end. Whenever the anode voltage is more positive than the cathode voltage, the diode is described as having a forward-bias, and it conducts with a relatively low-voltage drop. Similarly, when the cathode voltage is more positive than the anode, the diode is said to have a reverse-bias [39].1N4148is used in the bootstrap circuit ,and HBR20100 in buck converter. Figure 4.7 demonstrate both diodes

- **Capacitors:**A capacitor is a passive electronic component with two terminals. It consists of two conductive plates separated by an insulating material called a dielectric. The size of the conductive plates and the permittivity of the insulating dielectric material deter-

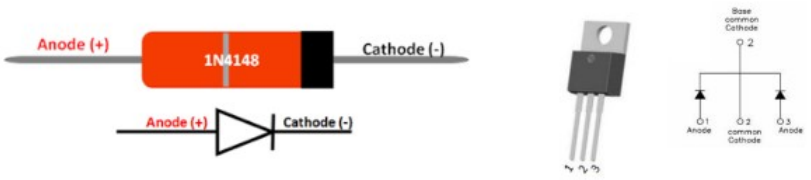

Figure 4.7: 1N4148 and HBR20100 diode

mine capacitance, which is the amount of charge that can be stored at a given voltage by a capacitor. The unit of capacitance is the Farad (F) and a 1F capacitor charged to 1V will hold one Coulomb of charge.Capacitors are used in a variety of applications, including energy storage, filtering, timing, and voltage regulation [39]. The used capacitors: two of$330\mu F$,$220\mu F$,four of$100\mathrm{p}F$and one of$10\mu F$.

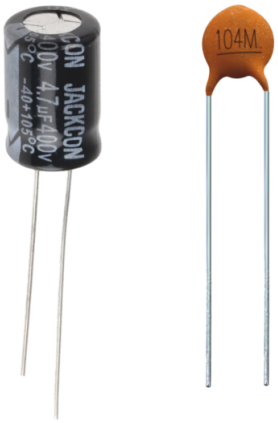

Figure 4.8: ceramic and electrolytic capacitor

4.9 The Implemented PWM Signal:

In simulation the buck converter diode was replaced by a MOSFET.This configuration is known as the synchronous buck converter and have the same behavior as the conventional buck converter when the high side MOSFET is ON. But when the high side switch is OFF ,the low side MOSFET turns ON and starts conducting to provide a path for the inductor current to be discharged. This topology was chosen to take full advantage of the driver PWM signals ;because the control circuit synchronize the timing of both MOSFETs with the switching frequency and it has a higher efficiency with faster switch turn-on time [40].

Figure 4.9 show the PWM signals delivered to both the MOSFET's at duty cycle equal to D=65% .The violet signal is for the HIGH side MOSFET while the blue one is for the LOW side MOSFET . And figure 4.10 present the bootstrap circuit of the driver.

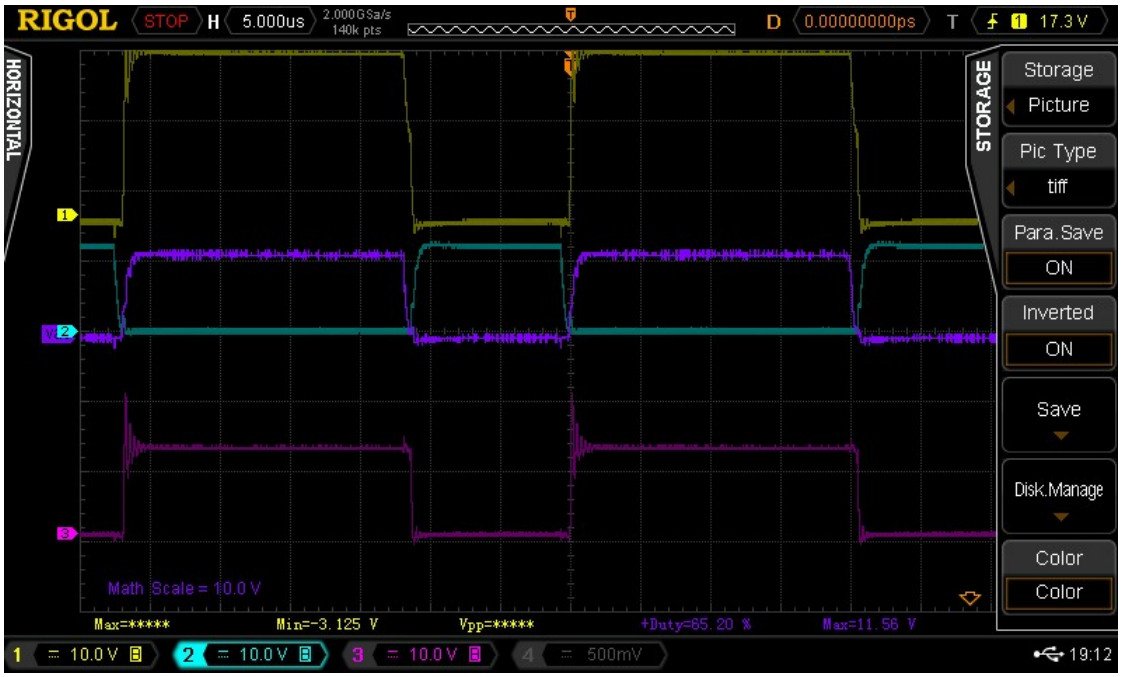

Figure 4.9: PWM signals at D=65%

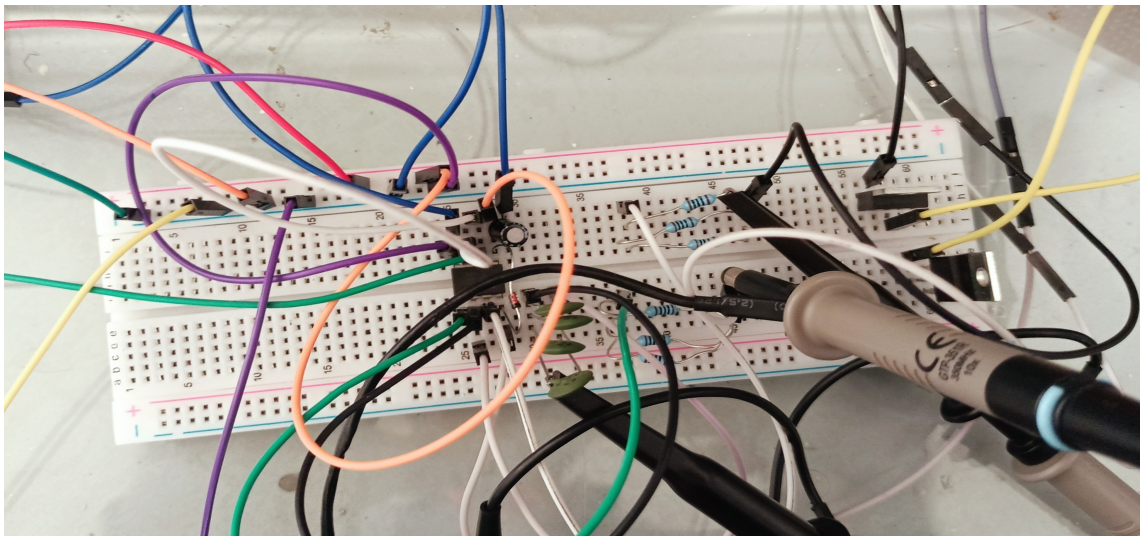

Figure 4.10: Implemented bootstrap circuit for the driver

4.10 Hardware Implementation of Buck Converter :

The DC-DC converter is implemented as shown in figure4.11.

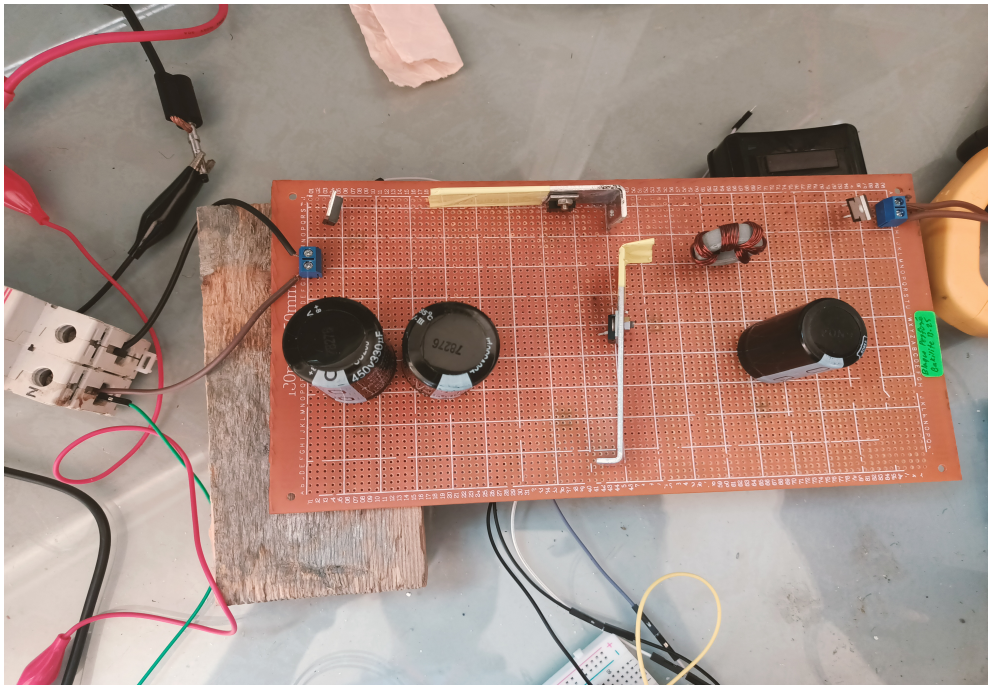

Figure 4.11: Implemented buck converter

The test was run with no MPPT mode,it was seen when no MPPT algorithm is used the power delivered to the load was low(8.28W) compared to the power generated either by the voltage emulator or the PV panel(18V*1.2A=21.6W).This is due to many factors such as the power loss in the power circuit for the lack of high precision in building the circuit , also for not varying the duty cycle of the converter by the MPPT algorithm ,and the day that the test was performed was cloudy day therefore the irradiance was very week .

Figure 4.12 demonstrate the complete hardware setup .

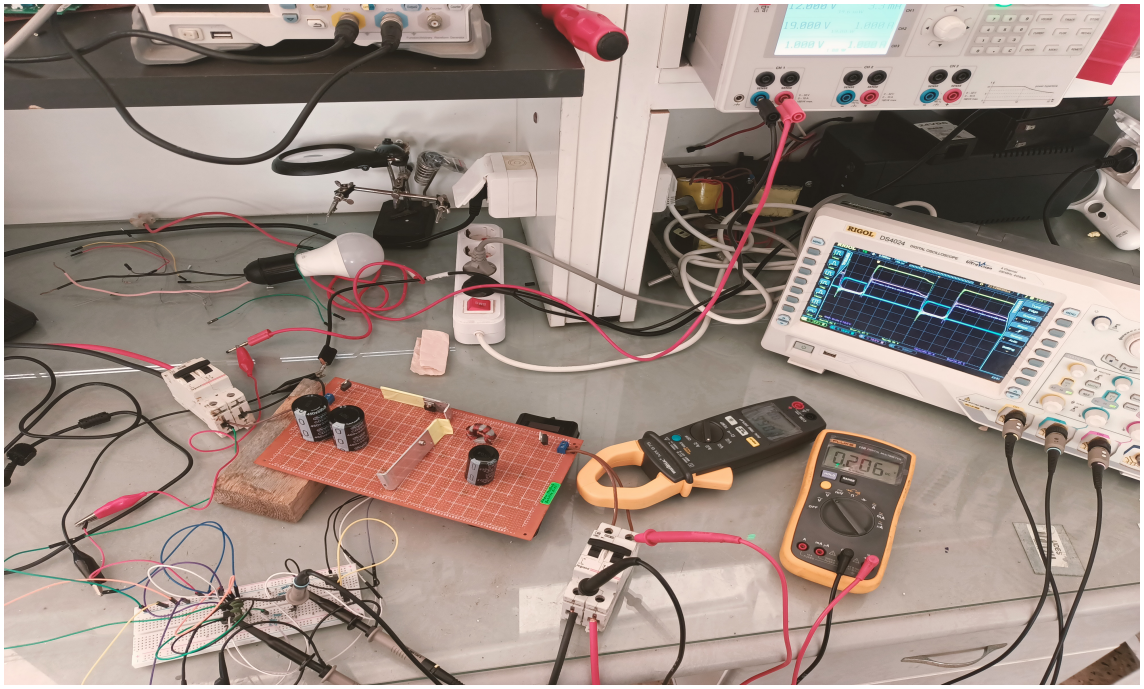

Figure 4.12: Complete hardware setup without PV panel

4.11 Conclusion:

This chapter has highlighted the components used to implement the PV system and the importance for selecting the suitable components for the best results;and also it has shown the implemented circuits of both the buck converter and the driver circuit that controls the switches. Finally, it has presented the complete hardware setup .

General Conclusion:

In this research, a Photovoltaic system is presented to charge a battery. The main focus of this research were how to improve the total system efficiency by implementing an efficient MPPT technique to extract the maximum available power from PV panels under changing atmospheric conditions.

The four propose MPPT algorithms P&O, IC, FOCV, and FSCC are simulated and tested using MATLAB/SIMULINK. The performances of the proposed algorithms were compared under standard conditions and under changing irradiance and temperature levels. The comparative study considers three important features: the maximum power point tracking speed, steady state oscillations to find the average extrated power, and the real maximum power point to calculate the efficiency. The simulation relsults showed that the P&O and IC have approximately the same tracking speed with IC been the more efficient compared to FOCV and FSCC under standard conditions. However, under changing irradiance and temperature levels the IC tends to take the lead in every aspect noting that the FOCV and FSCC algorithms took the lead in the final scenario. A charging control condition is added to prevent the battery from been overcharged. The results were presented in order to show the performance and functionality of the system.

The implementation part of the proposed PV system was designed and tested using Proteus for its ability to approximate the simulation to the real-life performances it validate the functionality of the used Arduino code for P&O.

There were some limitations that presented an obstacles in simulation and implementation such as: the restricted list of materials, the provided Proteus version did not contain a real time curve plotting tool to show the Power curve versus time(P(t)) nor to extract the current

and voltage values. Additionally, Proteus has a very low sampling time so it could take hours just to simulate few seconds.

For further work, a snubber circuit can be used to eliminate noise and parasitic effects, resulting in better performance and accuracy. Improve the algorithms to enhance stability and fast tracking capabilities under different conditions. Another improvement can be achieved by designing a charge controller specifically for the battery. After implementing these enhancements, a PCB will be designed.

Bibliography:

- **[1]** S. J. Fonash, S. Ashok, and R. T. Fonash, ”Solar Cell,” Encyclopaedia Britannica, 2023. [Online]. Available: https://www.britannica.com/technology/solar-cell. [Accessed: Apr. 15, 2023].
- **[2]** Electrical4U, ”Solar Cell: Working Principle & Construction (Diagrams Included),” Electrical4U, 2020. [Online]. Available: https://www.electrical4u.com/solar-cell/. [Accessed: Apr. 15, 2023].
- **[3]** ”Solar Cell, module, array,” Samlex Solar, 2015. [Online]. Available: https://www.samlexsolar.com/learning-center/solar-cell-module-array.aspx. [Accessed: Apr. 15, 2023].
- **[4]** Rodrigues, E., Melício, R., Mendes, V. and Catalão, J. (2011) Simulation of a Solar Cell Considering Single-Diode Equivalent Circuit Model. Renewable Energies and Power Quality Journal, 1, 369-373, doi: 10.24084/repqj09.339
- **[5]** M. G. Villalva, J. R. Gazoli and E. R. Filho, ”Modeling and circuit-based simulation of photovoltaic arrays,” 2009 Brazilian Power Electronics Conference, Bonito-Mato Grosso do Sul, Brazil, 2009, pp. 1244-1254, doi: 10.1109/COBEP.2009.5347680.
- **[6]** N. Singh and A. Goswami, ”Study of P-V and I-V Characteristics of Solar Cell in MATLAB/Simulink,” International Journal of Pure and Applied Mathematics, vol. 118, no. 24, 2018.
- **[7]** Electrical Technology, ”Parameters and Characteristics of a Photovoltaic Cell,” Electrical Technology, 2020. [Online]. Available: https://www.electricaltechnology.org/2020/09/parameters-characteristics-solar-panel.html. [Accessed: Apr. 15, 2023].

- **[8]** Alternative Energy Tutorials, "Solar Cell I-V Characteristic," Alternative Energy Tutorials, 2020. [Online]. Available: https://www.alternative-energy-tutorials.com/photovoltaics/solar-cell-i-v-characteristic.html. [Accessed: Apr. 15, 2023].
- **[9]** A. F. Mirza, M. Mansoor, Q. Ling, M. I. Khan, and O. M. Aldossary, "Advanced Variable Step Size Incremental Conductance MPPT for a Standalone PV System Utilizing a GA-Tuned PID Controller," MDPI, Energies, vol. 13, no. 16, 2020. doi: 10.3390/en13164153.
- **[10]** W. Xiao, A. Elnosh, V. Khadkikar, and H. Zeineldin, "Overview of maximum power point tracking technologies for photovoltaic power systems," in IECON 2011-37th Annual Con- ference of the IEEE Industrial Electronics Society. IEEE, 2011, pp. 3900–3905.
- **[11]** M. Abdel-Salam, M.-T. EL-Mohandes, and M. Goda, "History of maximum power point tracking," Modern Maximum Power Point Tracking Techniques for Photovoltaic Energy Systems, pp. 1–29, 2020.
- **[12]** aerl, "THE HISTORY OF AERL AND THE MPPT SOLAR CHARGE CONTROLLER," aerl, 2022, . [Online]. Available: https://www.aerl.com.au/mppt- solar-charge-controller-history/. [Accessed: Mai 05 2023].
- **[13]** M. L. Katche, A. B. Makokha, S. O. Zachary, and M. S. Adaramola, "A comprehensive review of maximum power point tracking (mppt) techniques used in solar pv systems," Energies, vol. 16, no. 5, p. 2206, 2023.
- **[14]** A. D. Hansen, P. Sorensen, L. H. Hansen, H. Bindner et al., "Models for a stand-alone pv system," Roskilde: Rio National Laboratory, 2000.
- **[15]** . Khatib, I. A. Ibrahim, and A. Mohamed, "A review on sizing methodologies of photo- voltaic array and storage battery in a standalone photovoltaic system," Energy Conversion and Management, vol. 120, pp. 430–448, 2016.
- **[16]**. Knopf, "Analysis, simulation, and evaluation of maximum power point tracking (mppt) methods for a solar powered vehicle," Ph.D. dissertation, Portland State Univer-

sity Port- land, 1999.

- **[17]** lectricaltechnology, “Buck Converter – Circuit, Design, Operation and Exam- ples,” electricaltechnology, 2012, . [Online]. Available: https://www.electricaltechnology.org /2020/09/buck-converter.html . [Accessed: Mai. 06, 2023]
- **[18]** Dr.Taufik, “Practical Design of Buck Converter,” DOCPLAYER, . [Online]. Available: https://docplayer.net/30370591-Practical-design-of-buck- converter.html . [Accessed: Mai, 06. 2023]
- **[19]** S. D. Zainal, “Utjmb,” Power Electronics and Drives (Version 3-2003) ,Chapter 3 DC-DC Converter (CHOPPER), 2003.
- **[20]** M. S. Rahman, “Buck converter design issues,” 2007.
- **[21]** . Manimekalai, R. Harikumar, and S. Raghavan, “An overview of batteries for photovoltaic (pv) systems,” International Journal of Computer Applications, vol. 82, no. 12, 2013.
- **[22]** . Jossen, J. Garche, and D. U. Sauer, “Operation conditions of batteries in pv applications,” Solar energy, vol. 76, no. 6, pp. 759–769, 2004.
- **[23]** LibreTexts Chemistry, ’Batteries and Fuel Cells,’ LibreTexts Chemistry,[Online]. Available :https://chem.libretexts.org/Bookshelves/GeneralC hemistry/Chemistry1e(OpenSTAX)/17 . [Accessed: May 08, 2023].
- **[24]** . Adams, “Bootstrap componet selection for control ic’s,” [Online].Available : http://www. irf. com/technical- info/designtp/dt98-2. pdf, 2001.
- **[25]** . Diallo and H. P. Drivers, “Bootstrap circuitry selection for half-bridge configurations,” Application Report No. SLUA887. High Power Drivers Group, Texas Instruments: Dallas, TX, USA, 2018.

- **[26]** IXYS Corporation, "IX2127 Design Considerations Application Note: AN-400/INTEGRATED CIRCUITS DIVISION," IXYS Corporation, [Online].Available : https://datasheet.datasheetarchive.com/originals/crawler/claremicronix.com/492df790dccc7041bf807655cdcad793.pdf. [Accessed: May 08, 2023].
- **[27]**. N. Ali, K. Mahmoud, M. Lehtonen, and M. M. Darwish, "An efficient fuzzy-logic based variable-step incremental conductance mppt method for grid-connected pv systems," Ieee Access, vol. 9, pp. 26 420–26 430, 2021.
- **[28]** V. Banu, R. Beniug a, and M. Istrate, "Comparative analysis of the perturb-and-observe and incremental conductance mppt methods," in 2013 8Th International Symposium on advanced topics in electrical engineering (ATEE). IEEE, 2013, pp. 1–4.
- **[29]** . K. Yadav, S. Jha, and B. Kumar, "Comparative study of different variable step size perturb and observe based mppt," in 2020 International Conference on Advances in Com- puting, Communication Materials (ICACCM). IEEE, 2020, pp. 272–277.
- **[30]** M. Asim, M. Tariq, M. Mallick, I. Ashraf, S. Kumari, and A. K. Bhoi, "Critical evaluation of offline mppt techniques of solar pv for stand-alone applications," in Advances in Smart Grid and Renewable Energy: Proceedings of ETAEERE-2016. Springer, 2018, pp. 13–21.
- **[31]** Arduino.cc, "Arduino UNO R3," Arduino.cc, [Online]. Available: https://docs.arduino.cc/hardware/uno-rev3. [Accessed: Mai . 08 ,2023] .
- **[32]** icrocontrollerslab, "Arduino PWM Tutorial: Generate Fix and Variable Fre- quency and Duty Cycle Signal," microcontrollerslab.com, (Accessed:mai 06 2023) . [Online]. Available: https://microcontrollerslab.com/arduino-pwm-tutorial-generate-fix- and-variable-frequency-signal/.
- **[33]** Allegro microsystems inc, "ACS712", 2010. [Online]. Available: https://pdf1.alldatasheet.com/datasheet-pdf/view/428383/ALLEGRO/ACS712.html.

- **[34]** BINARYTECHPRIME, “Module capteur de tension alternative ZMPT101B monophas e,” binarytech-dz.com. [Online]. Available: https://binarytech-dz.com/produit/ arduinoraspberry/autres-modules/module-capteur- de-tension-alternative-zmpt101b-monophase/. [Accessed: Mai, 08 .2023].
- **[35]** International Rectifier , “IR2104(S) (PbF) HALF-BRIDGE DRIVER No. PD60046-S,” 4/2/2004. [Online]. Available: https://pdf1.alldatasheet.com/datasheet-pdf/view/86635/IRF /IR2104.html .
- **[36]** Ritar, “RA12-100(12V100Ah).” [Online]. Available: https://www.ritarpower.com/uploads/ ueditor/spec/RA12-100.pdf.
- **[37]** Coil32, “Inductance calculation of a ferrite toroid coil,” coil32.net, 23 JANUARY 2015 . [Online]. Available: https://coil32.net/ferrite-toroid-core.html . [Accessed: Mai. 08 ,2023].
- **[38]** Whatls, “What is a resistor?” techtarget.com, December 2021 . [Online]. Available: https://www.techtarget.com/whatis/definition/resistor . [Accessed: Mai. 08, 2023].
- **[39]** . Braza, “A COMPLETE GUIDE TO DIODES,” circuitbasics.com/ . [Online]. Available: https://www.circuitbasics.com/what-is-a-diode . [Accessed: Mai. 08,2023] .
- **[40]** H. Eraydin and A. F. Bakan, “Efficiency comparison of asynchronous and synchronous buck converter,” in 2020 6th international conference on electric power and energy con- version systems (EPECS). IEEE, 2020, pp. 30–33 .